

# Lawrence Berkeley National Laboratory

## LBL Publications

### Title

Powdery mildew induces chloroplast storage lipid formation at the expense of host thylakoids to promote spore production.

### Permalink

<https://escholarship.org/uc/item/1pj4p8g7>

### Journal

The Plant Cell, 37(3)

### Authors

Xue, Hang

Jaenisch, Johan

Sasse, Joelle

et al.

### Publication Date

2025-03-05

### DOI

10.1093/plcell/koaf041

Peer reviewed

# Powdery mildew induces chloroplast storage lipid formation at the expense of host thylakoids to promote spore production

Hang Xue,<sup>1,\*</sup> Johan Jaenisch,<sup>1,\*</sup> Joelle Sasse,<sup>2,4</sup> E. Riley McGarrigle,<sup>1</sup> Emma H. Choi,<sup>1</sup> Katherine Louie,<sup>3</sup> Katharina Gutbrod,<sup>4</sup> Peter Dörmann,<sup>4</sup> Trent R. Northen,<sup>2,3</sup> Mary C. Wildermuth<sup>1,\*</sup>

<sup>1</sup>Department of Plant and Microbial Biology, University of California, Berkeley, CA 94720, USA

<sup>2</sup>Environmental Genomics and Systems Biology Division, Lawrence Berkeley National Laboratory, 1 Cyclotron Road, Berkeley, CA 94720, USA

<sup>3</sup>The DOE Joint Genome Institute, Lawrence Berkeley National Laboratory, 1 Cyclotron Road, Berkeley, CA 94720, USA

<sup>4</sup>Institute of Molecular Physiology and Biotechnology of Plants (IMBIO), University of Bonn, 53115 Bonn, Germany

\*Author for correspondence: [mwildermuth@berkeley.edu](mailto:mwildermuth@berkeley.edu)

<sup>†</sup>H.X. and J.J. contributed equally.

<sup>‡</sup>Present address: Department of Plant and Microbial Biology, University of Zurich, Zurich 8008, Switzerland.

The author responsible for distribution of materials integral to the findings presented in this article in accordance with the policy described in the Instructions for Authors (<https://academic.oup.com/plcell/pages/General-Instructions>) is: Mary C. Wildermuth ([mwildermuth@berkeley.edu](mailto:mwildermuth@berkeley.edu)).

## Abstract

Powdery mildews are obligate biotrophic fungi that manipulate plant metabolism to supply lipids to the fungus, particularly during fungal asexual reproduction when lipid demand is high. We found levels of leaf storage lipids (triacylglycerols, TAGs) are 3.5-fold higher in whole *Arabidopsis* (*Arabidopsis thaliana*) leaves with a 15-fold increase in storage lipids at the infection site during fungal asexual reproduction. Lipid bodies, not observable in uninfected mature leaves, were found in and external to chloroplasts in mesophyll cells underlying the fungal feeding structure. Concomitantly, thylakoid disassembly occurred and thylakoid membrane lipid levels decreased. Genetic analyses showed that canonical endoplasmic reticulum TAG biosynthesis does not support powdery mildew spore production. Instead, *Arabidopsis* chloroplast-localized DIACYLGLYCEROL ACYLTRANSFERASE 3 (DGAT3) promoted fungal asexual reproduction. Consistent with the reported AtDGAT3 preference for 18:3 and 18:2 acyl substrates, which are dominant in thylakoid membrane lipids, *dgat3* mutants exhibited a dramatic reduction in powdery mildew-induced chloroplast TAGs, attributable to decreases in TAG species largely comprised of 18:3 and 18:2 acyl substrates. This pathway for TAG biosynthesis in the chloroplast at the expense of thylakoids provides insights into obligate biotrophy and plant lipid metabolism, plasticity, and function. By understanding how photosynthetically active leaves can be converted into TAG producers, more sustainable and environmentally friendly plant oil production may be developed.

## Introduction

As obligate biotrophic pathogens, powdery mildews acquire nutrients supplied by living host cells to support their life cycle and have specialized strategies for maximizing the output of these tissues (Glawe 2008; Wildermuth et al. 2017). In the *A. thaliana*–*Golovinomyces orontii* interaction, the establishment of the fungal feeding structure, called a haustorium, occurs by 24 h post-inoculation (hpi). By 5 days post-inoculation (dpi), asexual reproductive structures called conidiophores form. These conidiophores contain chains of conidia which store energy in the form of lipid bodies and glycogen (Both et al. 2005; Micali et al. 2008). Thus, the fungal demand for nutrients is especially high during asexual reproduction. As a response to the nutritional demands, a metabolic switch occurs in the host infected leaves. Mature leaves are considered source tissues producing hexoses for transport to growing parts of the plant. However, powdery mildew infection induces localized signatures of mobilization of carbohydrates to the tissue underlying the fungal infection site, for

fungal acquisition (Clark and Hall 1998; Sutton et al. 1999; Fotopoulos et al. 2003; Swarbrick et al. 2006). Furthermore, localized transcriptome profiling using laser microdissection shows the expression of genes associated with enhanced glycolysis and respiration to be increased, while the expression of chlorophyll biosynthesis genes is decreased at the powdery mildew infection site, in support of a localized source to sink transition (Chandran et al. 2010). Analysis of powdery mildew genomes found reduced carbohydrate metabolism pathways but relatively complete fatty acid (FA) metabolism and utilization pathways, suggesting lipids may be a preferred nutrient (Liang et al. 2018). Consistent with this preference, an early study found enhanced lipid accumulation in powdery mildew infected cucumber leaves compared with uninfected leaves (Abood and Lösel 1989). Moreover, more recent studies indicate powdery mildew spore lipids incorporate host lipids. Jiang et al. (2017) found that introducing UcfatB, a fatty acid thioesterase that terminates FA elongation early, with C12:0, into *Arabidopsis* resulted in increased C12:0 FAs in both host leaves and powdery mildew spores. Direct lipid

Received December 15, 2023. Accepted February 26, 2025.

© The Author(s) 2025. Published by Oxford University Press on behalf of American Society of Plant Biologists.

This is an Open Access article distributed under the terms of the Creative Commons Attribution-NonCommercial-NoDerivs licence (<https://creativecommons.org/licenses/by-nc-nd/4.0/>), which permits non-commercial reproduction and distribution of the work, in any medium, provided the original work is not altered or transformed in any way, and that the work is properly cited. For commercial re-use, please contact [reprints@oup.com](mailto:reprints@oup.com) for reprints and translation rights for reprints. All other permissions can be obtained through our RightsLink service via the Permissions link on the article page on our site—for further information please contact [journals.permissions@oup.com](mailto:journals.permissions@oup.com).

transfer from the plant to the powdery mildew was then confirmed by tracking isotope-labeled lipid precursors from infected leaves into powdery mildew spores (Lee et al. 2024).

Microbial acquisition of host lipids has emerged as a common strategy across host–microbe systems, particularly for obligate biotrophs including human intracellular pathogens (Atella et al. 2009; Costa et al. 2018). For plant obligate biotrophs, the arbuscular mycorrhizal fungi (AMF) symbiosis in which AMF colonize plant roots, providing minerals to the plant host while acquiring host sugars and lipids is best studied (Luginbuehl et al. 2017; MacLean et al. 2017; Kameoka and Gutjahr 2022). AMF induce a specific shift in host lipid metabolism, catalyzed by enzymes specific to plants colonized by AMF, to yield 2-monoacylglycerols (2-MG), with C16:0 2-MGs preferred. While 2-MGs appear to be the likely final product transferred to AMF, this has not been verified, and it is possible other lipids may also be transported particularly if acquisition is facilitated by exocytotic vesicles. Once these host lipids are acquired, they are remodeled by the AMF and stored primarily as TAGs in lipid bodies for future use.

By contrast with the AMF symbiosis, little is known about how host FA synthesis and lipid assembly are manipulated for powdery mildew lipid acquisition. Because powdery mildews have the capacity to synthesize FAs, unlike AMF which are FA auxotrophs (Kameoka and Gutjahr 2022), we focus our studies on powdery mildew-infected leaves during powdery mildew asexual reproduction (5+ dpi), when conidia (aka spores) replete with lipid bodies are formed. We reason that host lipids would be most in demand at this phase of the powdery mildew life cycle. Furthermore, as described above, 2 separate lines of evidence indicate that powdery mildew spore storage lipids are derived from host-acquired lipids (Jiang et al. 2017; Lee et al. 2024).

Plant lipid metabolism is dynamic across developmental stages and responsive to environmental stimuli, modifying energy content of storage tissues, altering membrane fluidity at different temperatures, minimizing lipotoxicity, and providing chemical signals (Baud et al. 2008; Moellering et al. 2010; Okazaki and Saito 2014; Cavaco et al. 2021). In plants such as *Arabidopsis*, acyl-chains are produced in chloroplasts, with the exception of a small fraction generated in mitochondria, and their subsequent assembly into lipids occurs via pathways operating in the chloroplast (prokaryotic pathway) and the endoplasmic reticulum (eukaryotic pathway). In *Arabidopsis* leaves, approximately 38% of newly synthesized FAs are utilized in the prokaryotic lipid-synthesis pathway, whereas the remaining 62% are directed towards the eukaryotic pathway (Browse et al. 1986). A portion of acyl-chains from ER-assembled lipids are subsequently transported—likely as PA and/or DAG—back to the plastid to serve as substrates for thylakoid lipid synthesis (Hölzl and Dörmann 2019; Yao et al. 2023).

Triacylglycerols (TAGs), neutral storage lipids with three fatty acids attached to a glycerol backbone, are packaged into lipid bodies. Eukaryotes synthesize TAGs in the ER via 2 major pathways: the Kennedy pathway and the acyl-CoA independent pathway (Xu et al. 2020). Diacylglycerol acyltransferases (DGAT, EC 2.3.1.20) catalyze the final and rate-limiting step in TAG synthesis forming TAG from diacylglycerol (DAG) and acyl-CoA in the Kennedy pathway. Whereas, phospholipid:diacylglycerol acyltransferase (PDAT, EC 2.3.1.158) catalyzes the final and rate-limiting step in acyl-CoA independent TAG synthesis with TAG formed from DAG and a phospholipid (PL) acyl donor, i.e. phosphatidylcholine (PC) remodeled from the Lands Cycle (Dahlqvist et al. 2000; Zhang et al. 2009; Wang et al. 2012).

In this study, we show powdery mildew-induced TAG accumulation and lipid body formation in mature *A. thaliana* leaves occurs

at the infection site concurrent with powdery mildew asexual reproduction. Confocal and transmission electron microscopy indicate the induced chloroplast-produced lipid bodies bleb out of chloroplasts in mesophyll cells underlying the fungal haustorial complex. Integrated genetic, microscopic, and lipidomic approaches uncover a route for plant TAG synthesis via AtDGAT3 to support powdery mildew spore formation. DGAT enzyme classes (DGAT1, DGAT2, and DGAT3) are products of distinct evolutionary trajectories with functional convergence on DGAT activity (Turchetto-Zolet et al. 2011; Yin et al. 2022). While DGAT1 and DGAT2 are largely conserved across eukaryotes, DGAT3 is unique to Viridiplantae. DGAT3 is unusual in that, unlike the ER membrane proteins DGAT1 and DGAT2, it is a soluble metalloprotein containing a [2Fe-2S] cluster (Aymé et al. 2014). We show AtDGAT3 is localized to the chloroplast and responsible for powdery mildew-induced plastidic TAG synthesis that occurs at the expense of thylakoid membranes. We then speculate on functional roles of ER- versus chloroplast-derived lipid bodies in the powdery mildew interaction, powdery mildew acquisition of the chloroplast-derived lipid bodies, and controls over AtDGAT3 stability and activity. Our findings open further avenues of investigation with respect to biotroph–host interactions and plant response to stress or aging (e.g. leaf senescence). Moreover, this work could facilitate more sustainable production of vegetable oil, biofuels, and other specialty chemicals (Xu et al. 2018).

## Results

### Powdery mildew infection increases triacylglycerol content in the host leaf while phospholipids decrease

Powdery mildew fungi are obligate biotrophs that rely entirely on the host for nutrients. Powdery mildew asexual reproduction creates a high metabolic demand for lipids as the powdery mildew feeding structures, haustoria, and newly formed spores are filled with lipid bodies at 5 dpi when asexual reproduction is first apparent (Fig. 1, A to C).

To understand how host lipid metabolism is manipulated to meet this fungal lipid demand, we performed lipid profiling of uninfected (UI) non-inoculated and parallel powdery mildew-infected leaves at 12 days post-inoculation (dpi). This later time point exhibits sufficient powdery mildew proliferation to allow us to assess the impact of the powdery mildew in whole leaf analyses. Lipids were extracted and identified by LC-MS/MS fragmentation patterns (Supplementary Fig. S1, Supplementary Data Set 1). Our results show that TAGs increase in 12 dpi washed leaf extracts relative to uninfected leaf extracts, with a 3.5-fold increase in abundance (Fig. 1D). Overall, there is a shift to TAGs containing longer acyl chains, including very long chain fatty acids (VLCFA,  $\geq$ C20), assessed at  $\geq$ C56:x, which increase 7-fold with infection (Fig. 1, E and F, Supplementary Fig. S1A; Supplementary Data Set 1). Examination of the most abundant TAG class, C54:x, shows an increase of 3.5-fold with infection accompanied by a shift towards a more desaturated profile in infected leaves (Fig. 1, F and G); this reflects increased 18:3 and 18:2 FA composition (Supplementary Data Set 1). As 18:3 and 18:2 are enriched in thylakoid membrane lipids, we also examined 16:3, unique to the thylakoid membrane (Browse et al. 1986). Five TAG species were identified as uniquely containing a 16:3 acyl chain, and each of these TAGs also contains at least one 18:3 acyl chain. With infection, these C16:3 containing TAGs increase by 5.4-fold (Supplementary Fig. S1B).

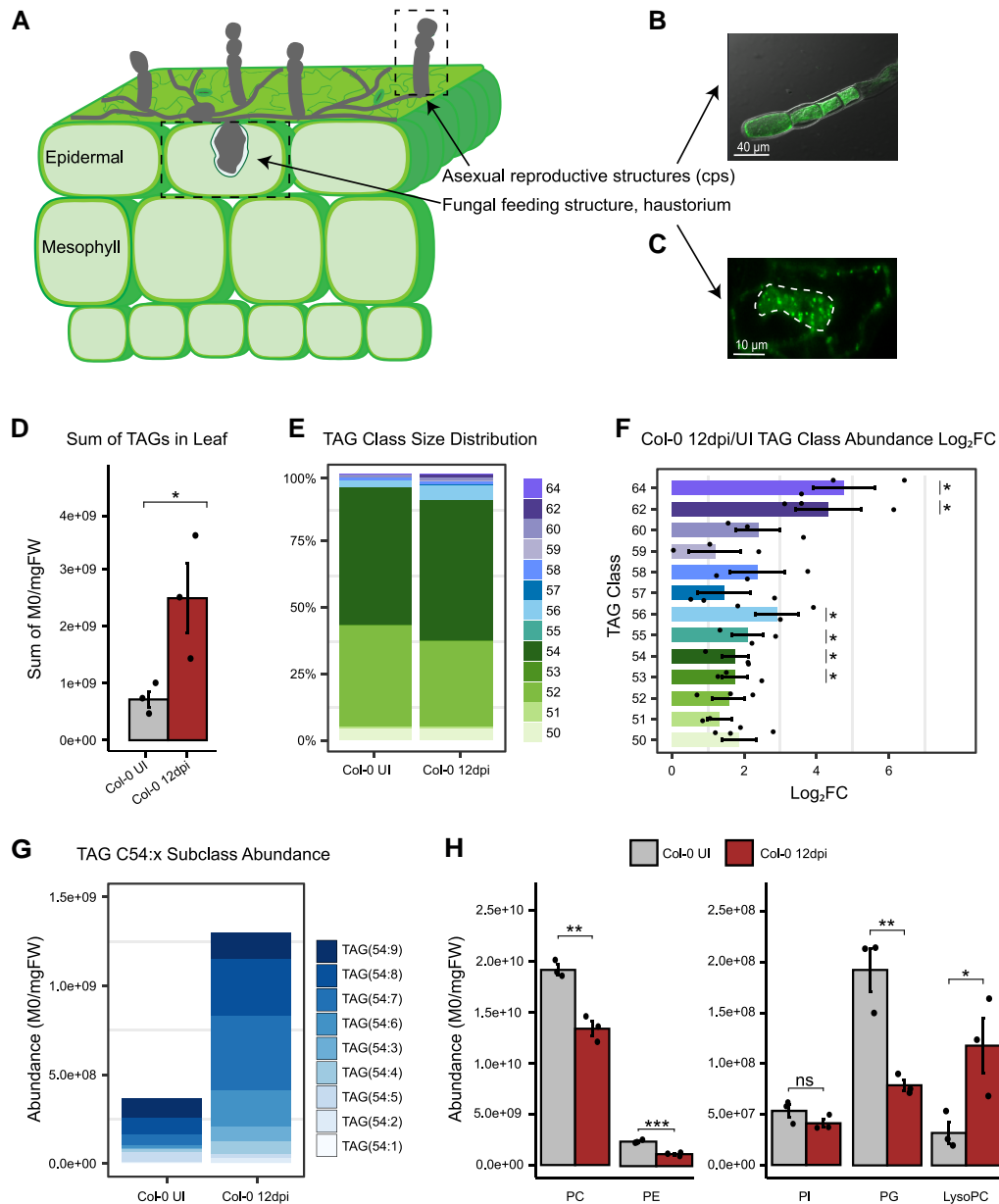


**Figure 1.** TAG abundance is increased in infected Col-0 leaves. **A)** Cross-section depicting powdery mildew infection of *Arabidopsis* leaf at 5 dpi. **B, C)** BODIPY 505/515 neutral lipid-stained powdery mildew structures: **B)** Asexual reproductive structure, conidiophore (cp), bar = 40  $\mu\text{m}$ . **C)** haustorium, bar = 10  $\mu\text{m}$ , white dashed line outlines haustorium. **D)** Total triacylglycerols (C50-C64) detected in UI and 12 dpi leaf lipid extracts, mean  $\pm$  SE,  $n = 3$  independent pools of leaves. **E)** Distribution of TAG classes in UI and 12 dpi leaf lipid extracts, mean  $\pm$  SE,  $n = 3$  independent pools of leaves. **F)**  $\text{Log}_2$  fold change ( $\text{Log}_2\text{FC}$ ) of TAG abundance by class in 12 dpi vs UI leaf lipid extracts, mean  $\pm$  SE,  $n = 3$  independent pools of leaves. **G)** Abundance of C54:x subclasses in UI and 12 dpi leaf lipid extracts. Assumes TAGs within this  $m/z$  range have similar desorption/ionization properties. **H)** Summed abundance of detected phospholipids (M0/mgFW) in UI and 12 dpi leaf lipid extracts, mean  $\pm$  SE,  $n = 3$  independent pools of leaves. In above panels, significance between UI and 12 dpi tested by unpaired, two-tailed Student's T-test, \* $P \leq 0.05$ , \*\* $P \leq 0.01$ . Abbreviations: dpi, days post inoculation; FW, fresh weight; LPC, lysophosphatidylcholine; M0, monoisotopic mass; PC, phosphatidylcholine; PE, phosphatidylethanolamine; PG, phosphatidylglycerol; PI, phosphatidylinositol; TAG, triacylglycerol; UI, uninfected non-inoculated.

While TAG amounts increase, phospholipids decrease in abundance in extracts from infected leaves at 12 dpi compared with parallel uninfected leaves (Fig. 1H, Supplementary Data Set 1). Phosphatidylcholine (PC), the dominant phospholipid in mature *Arabidopsis* leaves, decreases by 30%. Phosphatidylethanolamine (PE) and phosphatidylglycerol (PG) decrease by 50% and 60% respectively in infected leaves. Although a net decrease in total phosphatidylinositol (PI) with infection of 20% is observed, it is not statistically significant. Lysophosphatidylcholines (LPC) increase

by ~4-fold in infected leaves. The observed decrease in PC is consistent with increased TAG synthesis utilizing DAG formed from PC (and PA) via DGATs. The decreases in the other phospholipids (PE, PI, PG) may facilitate increased flux to TAG accumulation. Furthermore, the indication that LPC increases at 12 dpi suggests possible operation of the Lands Cycle using PDAT1. In summary, our data indicate that the powdery mildew remodels mature leaf host lipid metabolism to promote localized TAG accumulation.

## Genetic analyses indicate the canonical route for plant TAG synthesis in the ER hinders powdery mildew asexual reproduction while chloroplast-localized DGAT3 promotes it

We next examined the impact of genes encoding proteins catalyzing the final and rate-limiting step in canonical TAG biosynthesis in the ER (Vanhercke et al. 2019) on powdery mildew spore production, AtDGAT1 (At2g19450), AtDGAT2 (At3g51520), and AtPDAT1 (At5g13640), using Arabidopsis null mutants. In seed oil accumulation, AtDGAT1 and AtPDAT1 play dominant roles. A null mutant in AtDGAT1 shows a 30% reduction in seed TAGs, while RNAi silencing of PDAT1 in a *dgat1-1* background or DGAT1 in *pdat1-1* background results in 70% to 80% decreases in seed oil content (Katavic et al. 1995; Zhang et al. 2009). While it does not contribute to seed TAG accumulation, AtDGAT2, along with AtDGAT1 and AtPDAT1, can impact leaf TAG accumulation (Fan et al. 2013; Zhou et al. 2013). Furthermore, we explored the impact of ATP-binding cassette A 9 (ABCA9), demonstrated to import FA/acyl-CoA into the ER and to exhibit a 35% reduction in seed TAG accumulation in *abca9* null mutants (Kim et al. 2013). The ER-localized long-chain acyl-CoA synthetase 1 (LACS1) was also investigated because it acts on long chain and very long chain FAs (Lü et al. 2009), which we observed to increase with infection (Fig. 1, E and F) and is the only ER-localized LACS (Zhao et al. 2010) with enhanced expression at the powdery mildew infection site at 5 dpi (Chandran et al. 2010).

To our surprise, *dgat1-1* and *abca9-1* mutants allow for enhanced powdery mildew spore production compared to wild type (WT) plants; whereas, the *lacs1-1*, *dgat2-1*, and *pdat1-2* mutants show no significant change in spore production (Fig. 2A). Assessment of independent null mutants in DGAT1 (*dgat1-2*) and ABCA9 (*abca9-3*) provide confirmation (Fig. 2A). Taken together, our findings indicate that TAG synthesis in the ER, using the FA importer ABCA9 and the TAG biosynthetic enzyme DGAT1, is not used to support powdery mildew spore production, but instead hinders it.

While AtDGAT1 and AtDGAT2 are ER-localized and membrane-bound, the third Arabidopsis DGAT protein, AtDGAT3, contains a predicted N-terminal chloroplast transit peptide (cTP) and no transmembrane domain (Aymé et al. 2018). AtDGAT3 was initially shown to be localized to the cytosol (Hernández et al. 2012), but that study utilized an N-terminus truncated form of the enzyme lacking the cTP. While acquiring and creating null mutants in AtDGAT3, we performed knockdown of AtDGAT3 via spray-induced gene silencing (SIGS) using dsRNA specifically targeting AtDGAT3. SIGS against DGAT3 results in >40% decrease in spore production compared to buffer control (Fig. 2B) and is associated with ~60% reduction in AtDGAT3 expression (Methods; Supplementary Fig. S2). To further assess the impact of DGAT3 on powdery mildew asexual reproduction, we obtained a homozygous null mutant with a T-DNA insertion in AtDGAT3, *dgat3-2* (Supplementary Fig. S3A). In addition, we generated CRISPR/Cas9-induced mutants, *dgat3-3.1* and *dgat3-3.2*, which contain a single-nucleotide insertion in the second exon, resulting in a frame shift and early stop codon (Supplementary Fig. S3B). *dgat3-2*, *dgat3-3.1*, and *dgat3-3.2* plants all exhibit reduced spore production compared to WT (Fig. 2B). The larger impact on spore production shown with SIGS of DGAT3 compared with null mutants in DGAT3 may be due to genetic compensation through development in the null mutant plants. None of the *dgat3* mutant plants exhibit any obvious developmental or morphological phenotypes.

To determine the localization of AtDGAT3, we cloned the genomic DNA encoding the full length AtDGAT3 sequence with a C-terminus GFP sequence under the control of the CaMV 35S promoter (Supplementary Fig. S3C). Transient expression of AtDGAT3-GFP in *Nicotiana benthamiana* leaves via *Agrobacterium* (*Agrobacterium tumefaciens*) infiltration results in intense GFP fluorescence that is colocalized with chlorophyll autofluorescence, indicating DGAT3 is localized to chloroplasts (Fig. 2C).

Figure 2D places the tested players in the context of integrated chloroplast-ER lipid metabolism focused on TAG synthesis (Browse et al. 1986; Hölzl and Dörmann 2019; Vanhercke et al. 2019; Xu et al. 2020), with the addition of AtDGAT3 chloroplast localization. In summary, Arabidopsis leaf TAG synthesis to support powdery mildew asexual reproduction occurs via DGAT3 in the chloroplast. By contrast, canonical TAG synthesis in the ER via DGAT1 limits spore production.

## Powdery mildew-induced host lipid bodies are present both in the cytosol and chloroplasts

Given our finding that plastid DGAT3 supports powdery mildew spore production, we performed confocal imaging of infected leaf tissue at 5 and 10 dpi stained with the neutral lipid dye BODIPY505/515 and focused on mesophyll cells at the powdery mildew infection site. As Arabidopsis RPW8.2 is specifically targeted to the fungal extrahaustorial membrane (EHM), we infected Col-0 lines expressing RPW8.2-YFP with *G. orontii* to visualize the haustorium (Wang et al. 2009). The haustorium resides in the plant epidermal cell as depicted in Fig. 1A and is located above ~3 mesophyll cells (Fig. 3A). At the infection site at 5 dpi, we observe abundant lipid bodies (LBs) in the 3 mesophyll cells right underneath the haustorium and not in neighboring or distal mesophyll cells (Fig. 3B, Supplementary Fig. S4) or in parallel uninfected tissue (Fig. 3B). As the infection progresses to 10 dpi, the abundance of LBs increases in the neighboring mesophyll cells. The percent area with fluorescence shows a ~6-fold increase with infection at 5 dpi and ~15-fold increase with infection at 10 dpi (Fig. 3C). BODIPY505/515-stained LBs are mostly observed in association with chloroplasts. Closer examination using 3D reconstructions of multiple z-stacked confocal images shows that some LBs are fully embedded in the chloroplast while others appear to be emerging from the chloroplast (Fig. 3D). We refer to LBs within or partly within the chloroplast as chloroplast lipid bodies (CLB).

## Chloroplast TAG accumulation, but not host defense, is altered in *dgat3-2*

To directly assess whether DGAT3 impacts powdery mildew-induced TAG formation, we performed lipid extractions on mature whole leaves and chloroplasts isolated from mature whole leaves from uninfected and 12 dpi *dgat3-2* and WT plants. Using thin layer chromatography (TLC), we observe dramatically increased TAGs in whole leaf extracts from infected leaves compared with uninfected leaves (Fig. 4, A and B), in accordance with our lipid profiling results (Fig. 1D). However, on the whole leaf level, the TAG content does not differ significantly between *dgat3-2* and WT plants. In response to infection, a dramatic increase is also observed in isolated chloroplast TAG content (Fig. 4, A and B). Moreover, the isolated chloroplast TAG content from infected 12 dpi leaves is reduced by ~60% in *dgat3-2* compared with WT plants. Furthermore, the TAG TLC profile of isolated chloroplasts is enriched in TAGs with a higher R<sub>f</sub> than those from whole leaves, overlapping the extra virgin olive oil

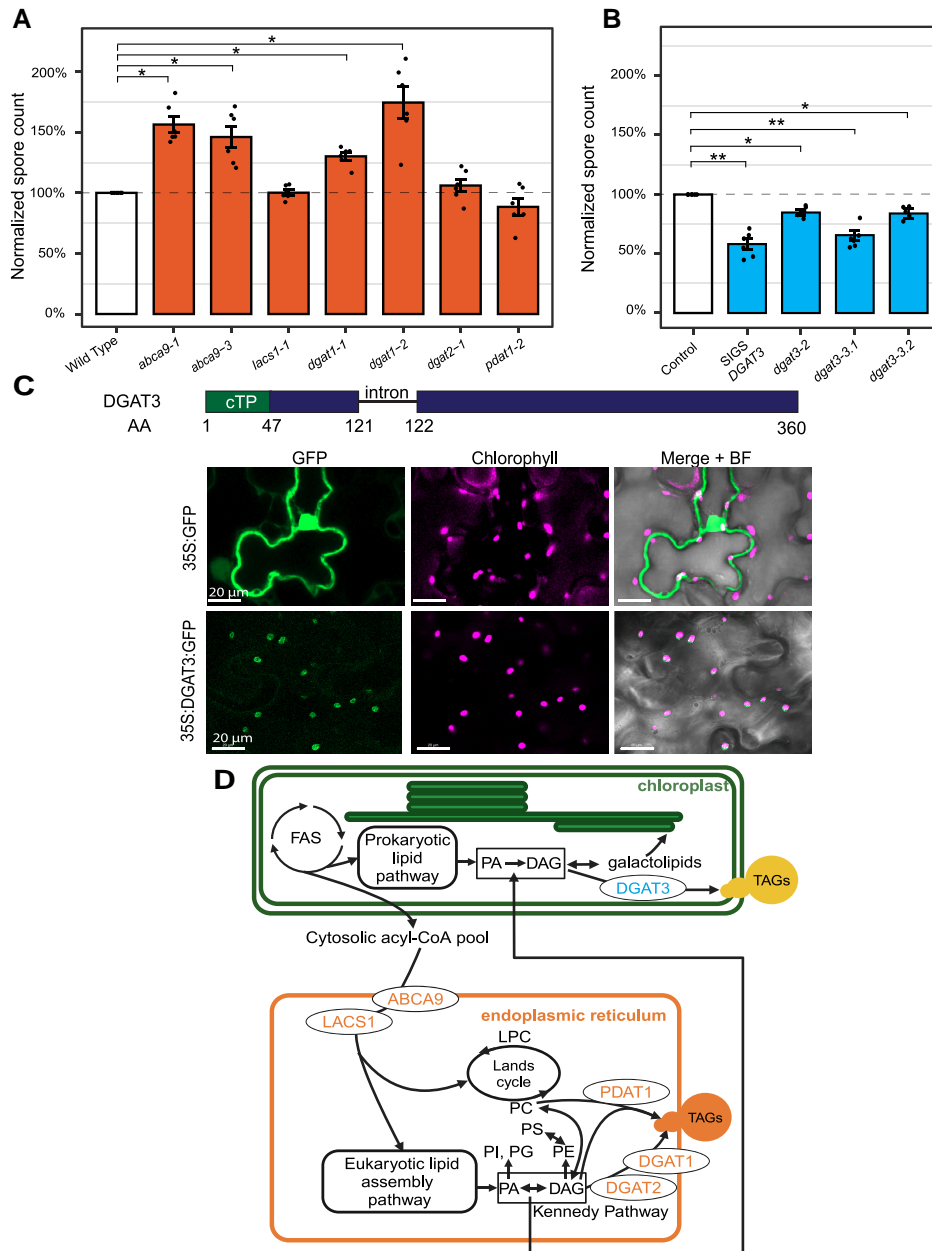


**Figure 2.** Canonical TAG synthesis in the ER hinders powdery mildew asexual reproduction while chloroplast-localized DGAT3 promotes it. **A)** Comparison of spore counts/mg leaf FW at 9 dpi for mutants involved in the canonical route for TAG synthesis in the ER normalized to parallel results for the appropriate WT ( $\pm$ SE,  $n = 5-8$  independent inoculation events). All mutants are in Col-0 ecotype except *dgat1-2* in WS. Significance by unpaired, two-tailed one-sample T-test,  $*P \leq 0.05$ . **B)** Comparison of spore counts/mg leaf FW at 9 dpi on WT plants with DGAT3 gene silenced via spray-induced gene silencing (SGS) and *dgat3* mutants vs. WT at 9 dpi ( $\pm$ SE,  $n = 6$  independent inoculation events). Significance by unpaired, two-tailed one-sample T-test,  $*P \leq 0.05$ ,  $**P \leq 0.01$ . **C)** AtDGAT3 protein is predicted to have a chloroplast transit peptide by the DeepLoc 2.0 and LOCALIZER programs. Confocal microscopy images of transient expression of 35S:AtDGAT3-GFP in *Nicotiana benthamiana*. **D)** Simplified model of tested players that may have contributed to Arabidopsis TAG production. Abbreviations: ABCA, ATP-binding cassette A; BF, bright field; Col-0, Columbia-0; cTP, chloroplast transit peptide; DAG, diacylglycerol; DGAT, diacylglycerol acyltransferase; dpi, days post inoculation; FAS, fatty acid synthase complex; FW, fresh weight; LACS, long chain acyl-CoA synthetase; LPC, lysophosphatidylcholine; PA, phosphatidic acid; PC, phosphatidylcholine; PE, phosphatidylethanolamine; PI, phosphatidylinositol; PS, phosphatidylserine; PDAT, phospholipid:diacylglycerol acyltransferase; TAG, triacylglycerol; WS, Wassilewskija; WT, wild type. See Fig. 1 for data on phospholipids.

standard (C18:1 74%, C18:2/3 11%, C16:0 15%). TLC analyses using another *dgat3* null mutant, *dgat3-3.1*, showed a similar result (Supplementary Fig. S5).

AtDGAT3 preferentially incorporates C18:3, and to a lesser extent C18:2, substrates into TAGs (Hernández et al. 2012; Aymé et al. 2018). To elucidate the differences in induced chloroplast TAG species composition between *dgat3* mutant and WT plants

at 12 dpi, we utilized the highly sensitive technique of direct infusion mass spectrometry (Gutbrod et al. 2021) of lipids extracted from these isolated chloroplasts. Among detected TAG classes, only the TAG 54:x class, the dominant TAG class in powdery mildew-infected leaves (Fig. 1E) exhibits a statistically significant difference in abundance (percent of total TAGs) for isolated chloroplasts from *dgat3-2* compared to WT plants at 12 dpi (Fig. 4C,

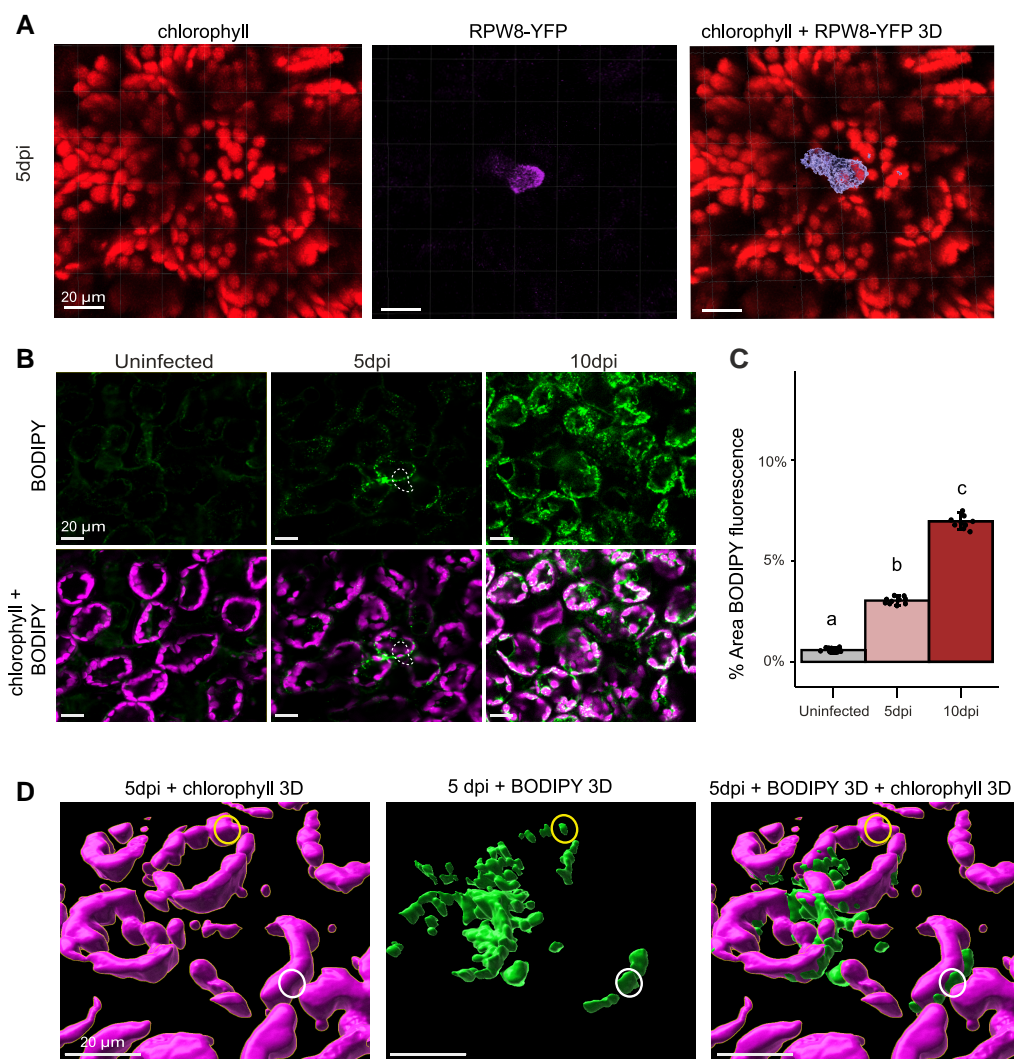


**Figure 3.** The powdery mildew induces the localized formation of lipid bodies in the host. **A)** Representative images of extrahaustorial membrane (EHM) targeted RPW8-YFP showing haustoria in epidermal cell above three mesophyll cells in rosette leaves at 5 days post inoculation (dpi). **B)** Representative images of BODIPY 505/515 staining of neutral lipids in mesophyll cell layers of rosette leaves at 5 and 10 dpi. White dash line: position of haustorium in the epidermal cell. **C)** Percentage of BODIPY fluorescence per image area of  $50,000 \mu\text{m}^2$  quantified by Imaris software. Data are mean  $\pm$  SE of 10 images. Means with different letters are significantly different according to one-way ANOVA followed by post-hoc Tukey test ( $P \leq 0.001$ ),  $n = 10$  chosen regions from two independent inoculation events. **D)** Representative images of 3D reconstruction of BODIPY fluorescence and chlorophyll fluorescence using Imaris software. Yellow circle: example BODIPY fluorescent body inside the chloroplast. White circle: example BODIPY fluorescent body emerging from the chloroplast.

Supplementary Data Set 2). TAG 54:x abundance as a percent of total TAGs in isolated chloroplasts is reduced by 54% in *dgat3-2* compared with WT. Within the TAG 54:x class, 3 individual TAG species, 54:9, 54:8, and 54:7, exhibit reduced abundance as a percent of total TAGs in infected isolated chloroplasts from *dgat3-2* compared with WT; reductions of 80%, 80%, and 60%, respectively, compared with WT are observed (Fig. 4D). TAGs 54:9, 54:8, and 54:7 contain 18:3 and 18:2 acyl chains that dominate thylakoid membranes and are the preferred substrates of DGAT3 (Hernández et al. 2012; Aymé et al. 2018). The only other TAG species that shows a statistically significant difference in percent abundance in isolated chloroplasts from *dgat3-2* versus WT is TAG 50:6 (most likely composed of 16:0, 16:3, and 18:3) with a 70% decrease in percent of total abundance (Supplementary Fig. S6).

Manipulation of plant lipid metabolism can result in altered defense signaling and response including elevated SA responses and/or cell death (Kachroo and Kachroo 2009) that restrict powdery

mildew growth and reproduction (e.g. Frye and Innes 1998; Reuber et al. 1998; Frye et al. 2001). Similar to WT, no cell death is observed in epidermal or mesophyll cells at the powdery mildew infection site of *dgat3-2* plants (Fig. 4E). Moreover, induced *pathogenesis-related gene 1* (PR1) expression, a marker of SA-dependent defense responses, does not differ between WT and *dgat3-2* in uninfected or infected leaves (Fig. 4F). Together, these findings suggest the reduction in spore production observed for *dgat3* mutants is due to decreased plastid TAG production, specifically in TAG species with mostly 18:2 and 18:3, and not to increased defense.

### Powdery mildew infection induces the breakdown of thylakoid membrane lipids

Above, we show powdery mildew-induced lipid bodies are associated with chloroplasts (Fig. 3) and plastid-localized AtDGAT3 is a dominant contributor to powdery mildew-induced host TAG

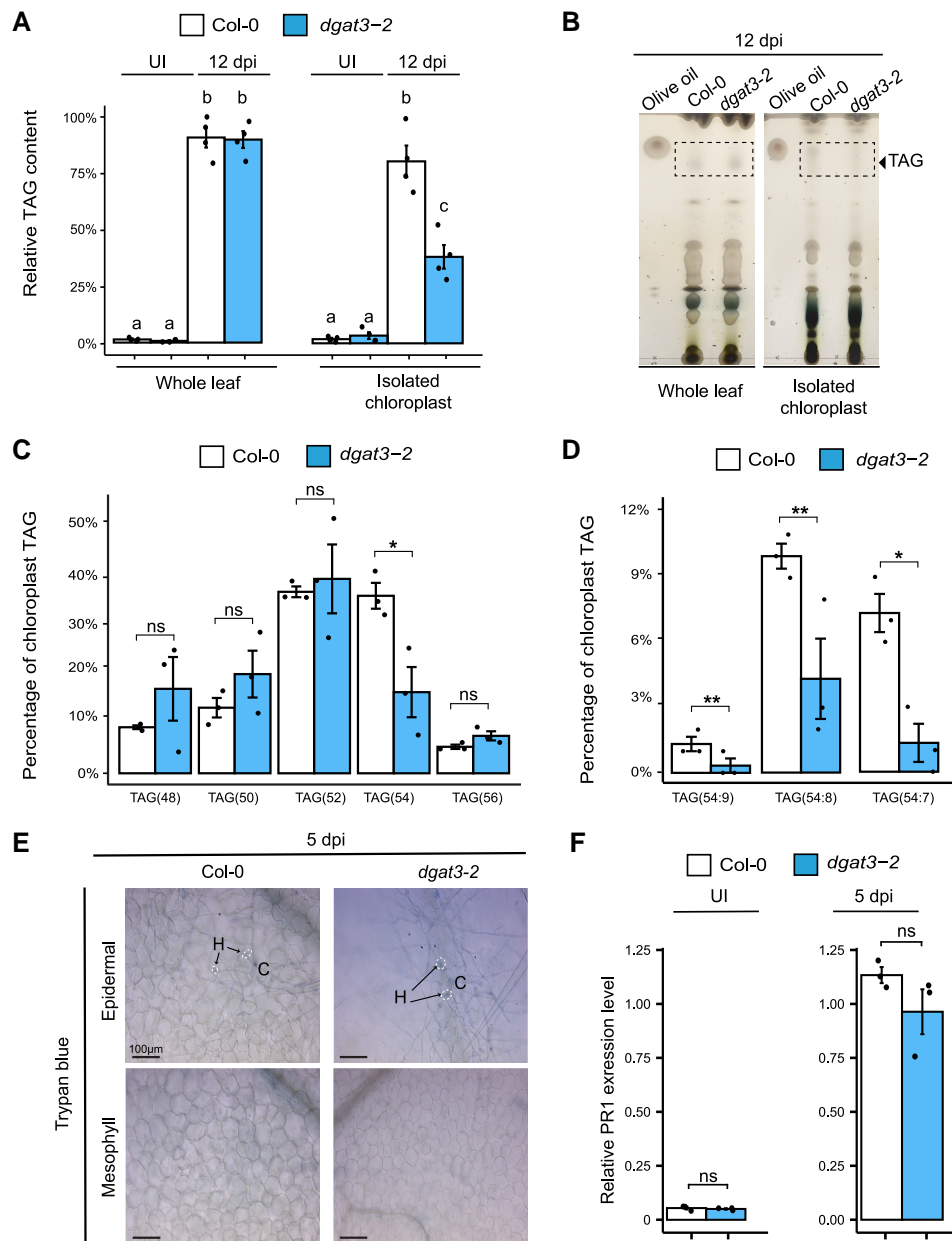


**Figure 4.** TAG content in chloroplasts from infected leaves is decreased in *dgat3-2* mutant while defense is not impacted. **A)** Relative TAG content in whole plants and chloroplasts of UI and 12 dpi Col-0 and *dgat3-2* were quantified by ImageJ software. Data are mean  $\pm$  SE of 4 independent pools of tissues. One-way ANOVA was performed on chloroplast samples and whole leaf samples separately. Means with different letters are significantly different according to one-way ANOVA followed by post-hoc Tukey test ( $P \leq 0.05$ ). **B)** Thin-layer chromatography of lipids extracted from either whole leaves or isolated chloroplasts. Lipids were visualized with 5% sulfuric acid by charring. **C)** Percentage of TAG class abundance in *dgat3-2* vs Col-0 chloroplast lipid extracts from leaves at 12 dpi; mean  $\pm$  SE,  $n = 3$  independent pools of tissues. Significance tested by unpaired, two-tailed Student's *T*-test,  $*P \leq 0.05$ . **D)** Percentage of TAG species (C54:9, C54:8 and C54:7) abundance in *dgat3-2* vs Col-0 chloroplast lipid extracts from leaves at 12 dpi; mean  $\pm$  SE,  $n = 3$  independent pools of tissues. Significance tested by unpaired, two-tailed Student's *T*-test,  $*P \leq 0.05$ ,  $**P \leq 0.01$ . **E)** Trypan blue staining to visualize cell death in Col-0 and *dgat3-2* plants at 5 dpi. Top panel, epidermal cell layer. Bottom panel, underlying mesophyll cell layer. Scale bar applies to all panels. H, haustorium; C, germinated conidium. Note that fungal structures are stained slightly by trypan blue. **F)** Quantitative real-time PCR (qRT-PCR) analysis of PR1 expression in UI and 5 dpi Col-0 and *dgat3-2* plants, normalized to housekeeping gene *ACTIN-2* (mean  $\pm$  SE,  $n = 3$  independent pools of tissues); significance determined using unpaired, two-tailed *T*-test. Abbreviations: Col-0, Columbia-0; DGAT3, diacylglycerol acyltransferase 3; dpi, days post inoculation; ns = not significant; PR1, pathogenesis-related gene 1; TAG, triacylglycerol; UI, uninfected non-inoculated.

synthesis that supports fungal spore production (Figs. 2 and 4). Furthermore, isolated chloroplasts from infected leaves largely contain TAGs with acyl chains enriched in thylakoid membranes, which are also the preferred substrates of DGAT3 (Hernández et al. 2012; Aymé et al. 2018), and isolated chloroplasts from

infected *dgat3-2* exhibit dramatic reductions in these TAGs (Fig. 4, C and D, Supplementary Data Set 2). Therefore, we postulated that host chloroplast membranes, dominated by thylakoid membranes, are being disassembled for TAG synthesis in response to infection.

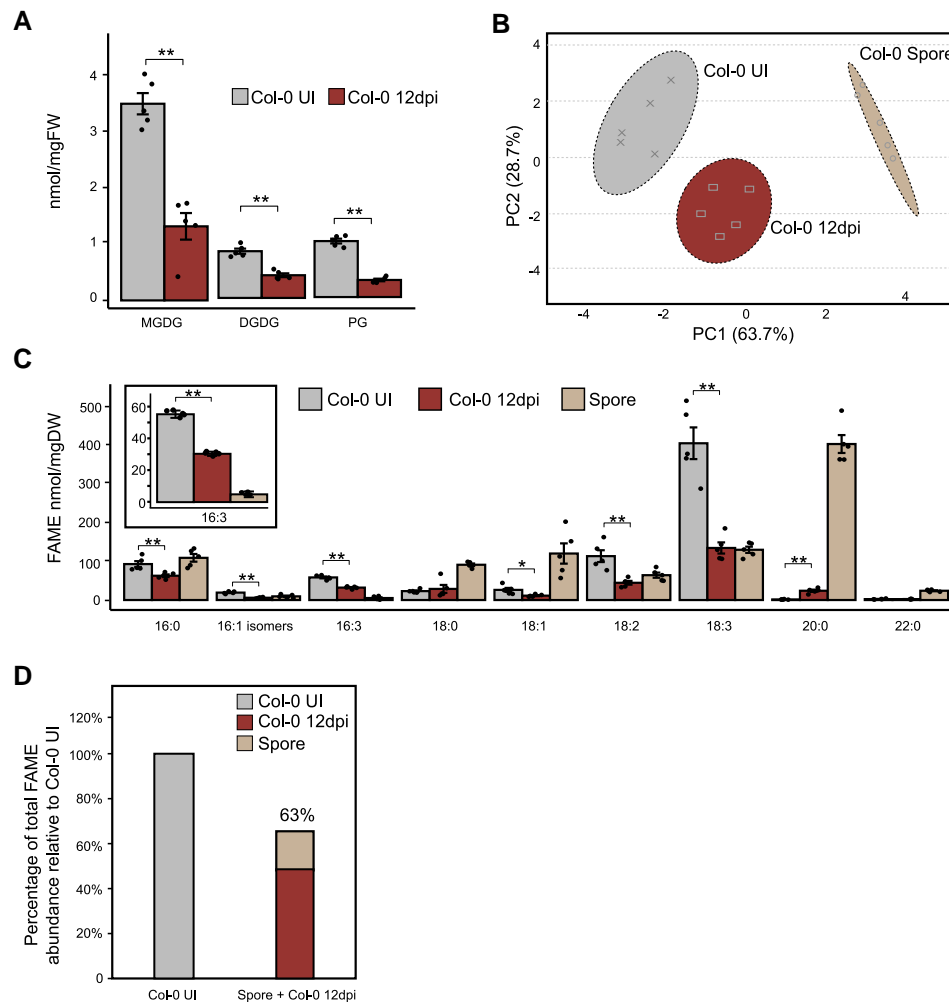


**Figure 5.** Thylakoid membrane lipids and thylakoid-enriched FAs decrease with infection. **A**) Abundance of thylakoid membrane lipids (MGDG, monogalactosyldiacylglycerol; DGDG, digalactosyldiacylglycerol; PG, phosphatidylglycerol) in UI and 12 dpi washed leaf lipid extracts (mean  $\pm$  SE,  $n = 5$  biological replicates). **B**) Principal component analysis plot based on abundance of FAME species detected (C16-C22) in Col-0 UI and 12 dpi washed leaf and spore lipid extracts,  $n = 5$  independent pools of tissues. **C**) Abundance of FA species detected in the same tissues as in **B**), normalized to mgDW of that tissue. **D**) Percentage of total FAME abundance in spore + Col-0 12 dpi washed leaf relative to Col-0 UI after conversion of spore data to nmol/mgDW leaf. Abbreviations: Col-0, Columbia-0; dpi, days post inoculation; DW, dry weight; FA, fatty acid; FAME, fatty acid methyl ester; FW, fresh weight; PC1, principal component 1; PC2, principal component 2; UI, uninfected non-inoculated.

We examined the abundance of thylakoid membrane lipids by electrospray ionization (ESI)-MS/MS. Uninfected mature *Arabidopsis* leaf thylakoid membrane lipids are dominated by monogalactosyldiacylglycerol (MGDG, 42%), digalactosyldiacylglycerol (DGDG, 13%), and phosphatidylglycerol (PG, 10%; [Browse et al. 1989](#)). Powdery mildew-infected (washed) whole leaves extracted at 12 dpi show that MGDG, DGDG, and PG each decrease by at least 2-fold compared to uninfected leaf controls indicating the breakdown of thylakoid membranes ([Fig. 5A](#), [Supplementary Data Set 3](#)). Decreased PG, by 60%, is also observed by LC-MS/MS ([Fig. 1H](#)).

To understand the change in total FA profiles, lipid extractions were performed on uninfected whole leaves, washed infected leaves, and spore tissues at 12 dpi. Acyl chains were then converted to fatty acid methyl esters (FAMES) for separation by gas chromatography with flame ionization detection (GC-FID). Principal component analysis (PCA) shows a distinct clustering of the 3 tissue types according to the 10 FA species detected ([Fig. 5B](#)). Acyl chains associated with thylakoid membrane lipids, C18:3 (dominant), C18:2, and C16:3 (unique to chloroplast), each

decrease by  $\sim$ 50% in 12 dpi compared with uninfected leaves ([Fig. 5C](#)). By contrast, the VLCFA C20:0 increases by  $\sim$ 20-fold in washed infected leaves. In spore extracts, the VLCFA C20:0 is the dominant species, followed by C18:3, while C18:3 dominates the leaf profiles even after the reduction shown with powdery mildew infection at 12 dpi. By normalizing the spore data to nmol/mgDW leaf ([Supplementary Data Set 3](#)), we can compare uninfected leaf total FA abundance with that of the washed leaves plus spores. We find 63% of total FA in the uninfected leaves is accounted for in the (washed) infected leaf plus spore ([Fig. 5D](#)). Moreover, only the spore C20:0 species abundance cannot be fully attributed to leaf acquisition as the spore contains 2-fold more C20:0 than the (washed) infected leaf and 36-fold more C20:0 than the uninfected leaf on a leaf normalized basis ([Supplementary Data Set 3](#)). This raises the possibility that some or most of the C20:0 in the (washed) infected leaf FAME samples and LC-MS/MS TAG samples ([Fig. 1](#), [Supplementary Data Set 1](#)) may be the result of fungal remodeling of host acquired lipids in the haustorial complex, as only the fungal haustorial complex remains in the washed leaf samples. Fungal remodeling of host

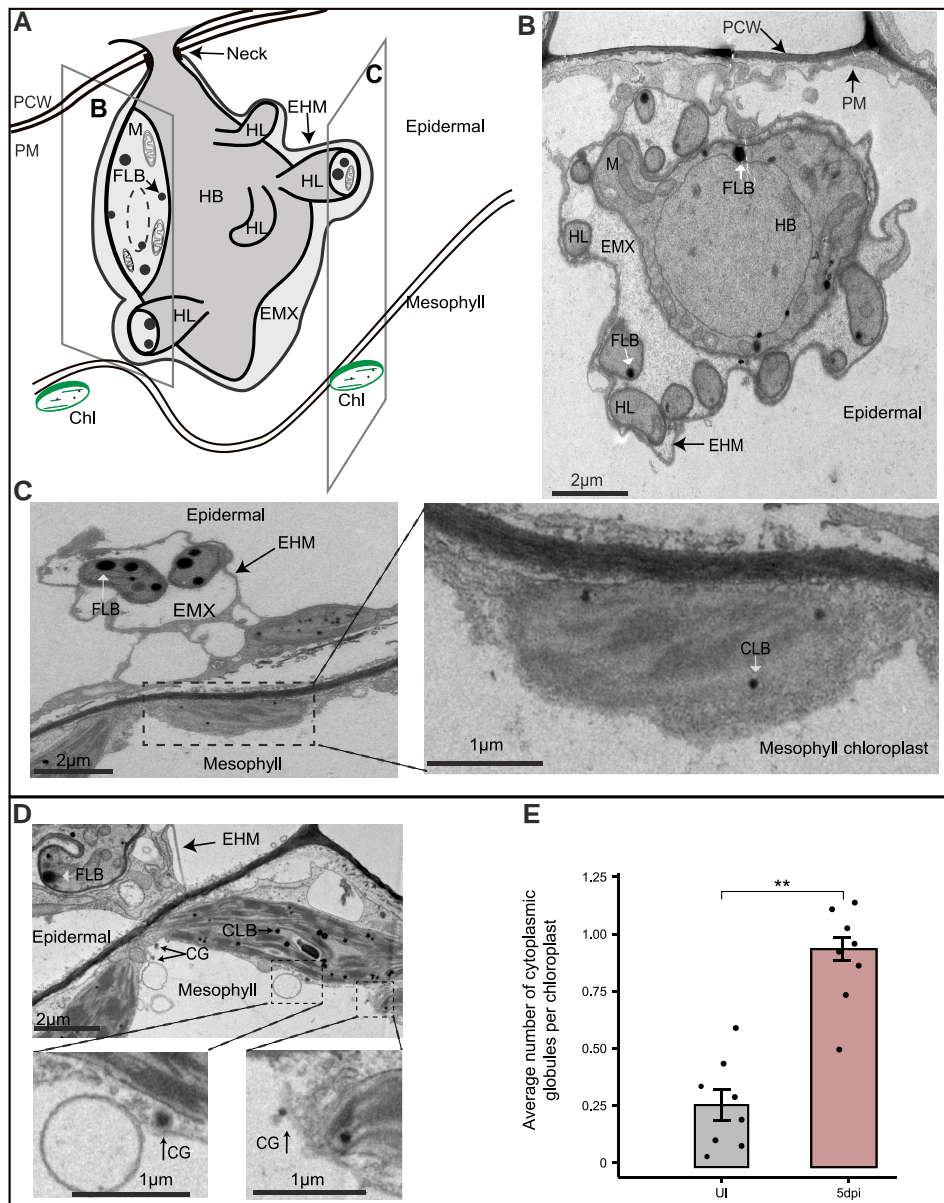


**Figure 6.** The powdery mildew induces the degradation of host chloroplasts and formation of cytoplasmic globules. **A)** 3D composite illustration of the *G. orontii* haustorium and underlying mesophyll cell chloroplasts at 5 dpi. **B)** Representative transmission electron microscopy (TEM) image centered on the haustorium. Note this slice does not include the haustorium neck. **C)** Representative TEM image showing mesophyll cell chloroplast associated with the haustorium and magnified mesophyll chloroplast. **D)** TEM image of haustorium and underlying mesophyll chloroplasts with prominent cytoplasmic globules. **E)** Average number of CGs per chloroplast (mean  $\pm$  SE,  $n=8$  biological replicates) for mesophyll cells underlying the haustorium-containing epidermal cell. Significance between UI and 5 dpi leaf samples: unpaired, two-tailed Student's T-test,  $*P \leq 0.05$ . Arrows highlight a specified cell component. Abbreviations: CG, cytoplasmic globule; Chl, chloroplast; CLB, chloroplast lipid body; dpi, days post inoculation; EHM, extrahaustorial membrane; EMX, extrahaustorial matrix; FLB, fungal lipid body; HB, haustorium body; HL, haustorium lobe; M, mitochondria; PCW, plant cell wall; PM, plasma membrane; UI, uninfected non-inoculated.

acquired lipids as opposed to de novo fungal synthesis of C20:0 is supported by isotope-tracking experiments in which host-derived lipid precursors were enriched in spore triacylglycerols including those with C20:0 acyl chains (Lee et al. 2024).

We next sought to examine whether there is an associated change in chloroplast substructures with infection. We examined the ultrastructures of the powdery mildew haustorial complex and underlying mesophyll cell chloroplasts at 5 dpi via transmission electron microscopy (TEM). Out of 18 prepared slices from 2 independent experiments, we obtained 6 independent slices with a visible haustorium. The mature haustorium consists of a

central haustorium body with peripheral small lobes (Koh et al. 2005). We see abundant electron-dense particles resembling LBs in the haustorium body and lobes, denoted as fungal lipid bodies (FLB), and CLBs in mesophyll cell chloroplasts underlying the haustorium-containing epidermal cell (Fig. 6). In 2 of the 6 slices, the mesophyll chloroplasts right underneath the haustorium show severe degradation, with chloroplast envelope membrane and thylakoid membranes almost totally degraded (Fig. 6C) compared with mesophyll chloroplast from a parallel uninfected leaf (Supplementary Fig. S7A). Although not all haustorium slices show obvious mesophyll chloroplast degradation, cytoplasmic

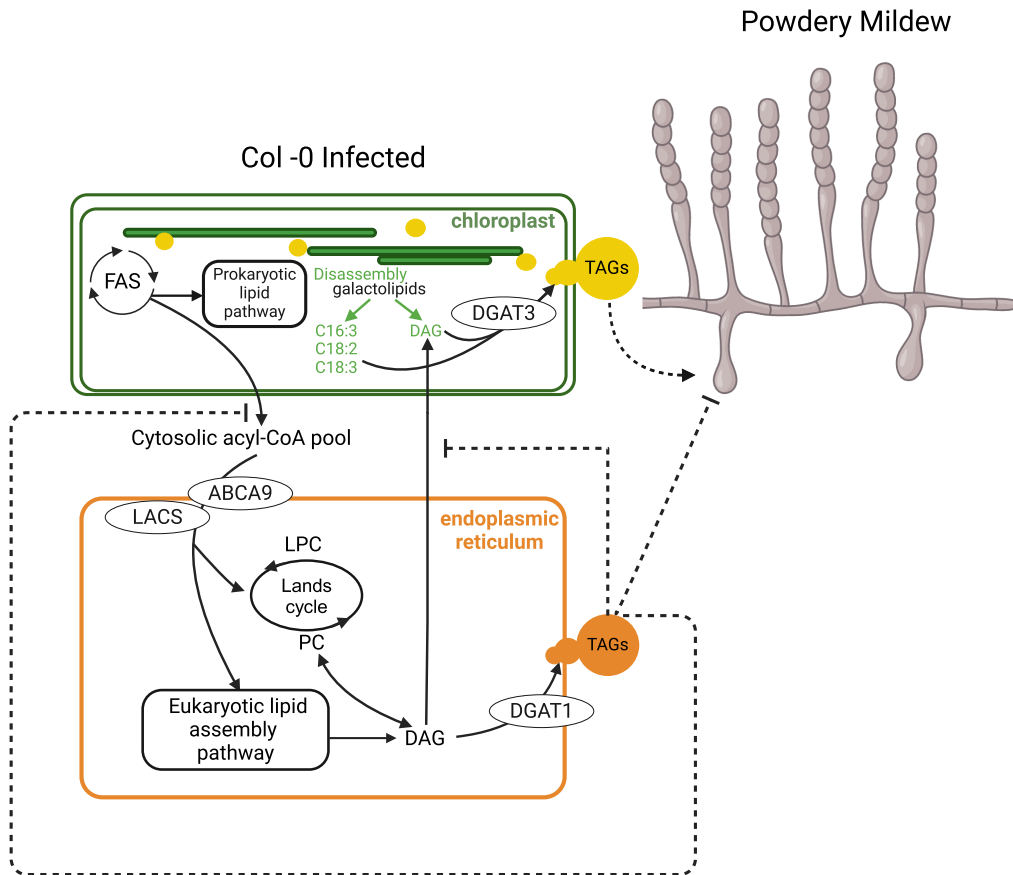


**Figure 7.** Infected *Arabidopsis* leaves have increased abundance of TAGs and chloroplast lipid bodies concurrent with degradation of thylakoid membranes. Confocal imaging suggests the chloroplast lipid bodies bleb into the cytosol (shown). And, TEM shows an increase in cytoplasmic globules per chloroplast and the potential for vesiculation of the chloroplast lipid bodies (not shown). Thylakoid lipids and derived fatty acids decrease with infection and are incorporated into accumulated TAGs. Plastid TAGs are mostly synthesized by chloroplast-localized AtDGAT3, which prefers C18:3 and C18:2 substrates, and have a unique profile compared to ER TAGs. Direct infusion MS of powdery mildew-induced TAGs from isolated chloroplasts shows decreased TAGs containing thylakoid membrane-derived acyl chains in *dgat3* compared to wild type. Knockdown of DGAT3 reduced powdery mildew spore production, indicating its function benefits the fungus, likely by supplying energy dense lipids for asexual reproduction and/or providing precursors for a fungal reproductive signal. In contrast, TAGs synthesized via DGAT1 in the ER hinder powdery mildew spore reproduction as assessed using knockouts in the ER fatty acid importer AtABCA9 and AtDGAT1. It is likely that multiple ER LACS activate imported FAs as a knockout in AtLACS1 alone was insufficient to alter powdery mildew spore production. AtPDAT1 and AtDGAT2, known to use a distinct ER DAG pool for TAG synthesis, do not contribute to powdery mildew asexual reproduction and are not included in the model. ER TAG synthesis via DGAT1 may reduce powdery mildew spore production by limiting substrates for plastid TAG synthesis and/or supplying lipid droplets that contain TAGs and defensive compounds. Abbreviations: ABCA, ATP-binding cassette A; DAG, diacylglycerol; DGAT, diacylglycerol acyltransferase; FAS, fatty acid synthase complex; LACS, long chain acyl-CoA synthetase; LPC, lysoPC; PC, phosphatidylcholine; PDAT, phospholipid:diacylglycerol acyltransferase; TAG, triacylglycerols. Dashed lines = proposed.

globules (CG) that appear to have been secreted from an associated chloroplast are observed in the 1 to 3 mesophyll cells right underneath the haustorium in all slices (e.g. Figure 6D, Supplementary Fig. S7B). These CGs have a similar electron density and size to the CLBs, 0.05 to 0.25  $\mu\text{m}$  and appear to have blebbed from the degrading chloroplast (Fig. 6, Supplementary Fig. S7). In some cases, the CGs are present in vesicles attached to the chloroplast membrane (Supplementary Fig. S7B). In total, the average number of CGs per chloroplast is 3.5-fold greater for mesophyll cells underlying the haustorium-containing epidermal cell compared with parallel uninfected leaf mesophyll cells (Fig. 6E). In addition, the number of starch granules per chloroplast is significantly reduced in the mesophyll cells right underneath the haustorium-containing cell compared to parallel uninfected leaf mesophyll cells (Supplementary Fig. S7C). Together, our data show that concurrent with *G. orontii* asexual reproduction (5 dpi+), powdery mildew infection induces the localized breakdown of host chloroplasts, as observed by TEM,

with decreased whole leaf thylakoid galactolipids and thylakoid membrane associated FAs in infected leaves.

## Discussion

### Powdery mildew-induced plastidic TAG synthesis via DGAT3 occurs at the expense of thylakoid membrane lipids

The powdery mildew-host plant system allows us to uncover a pathway for *Arabidopsis* TAG synthesis in the chloroplast. Figure 7 presents a simplified model showing chloroplast TAG synthesis via DGAT3 at the expense of thylakoid membranes supports powdery mildew asexual reproduction, incorporating our findings with the literature (Browse et al. 1986; Xu and Shanklin 2016; Hölzl and Dörmann 2019; Vanhercke et al. 2019; Xu et al. 2020; Bates 2022).

We analyzed the changes in *Arabidopsis* leaf lipids in response to powdery mildew infection at  $\geq 5$  dpi concurrent with the

formation of spores replete with lipid bodies (Fig. 1B). By 10–12 dpi, a 15-fold increase in neutral lipid fluorescence is observed in mesophyll cells underlying fungal feeding structures (Fig. 3B) with a 3.5-fold increase in TAG abundance at the whole leaf level (Fig. 1D). Localized thylakoid unstacking and degradation (Fig. 6), decreased thylakoid galactolipids (Fig. 5A), and associated FAs (Fig. 5C) suggest TAGs are formed at the expense of thylakoid lipids. This is confirmed by the increase in TAGs containing thylakoid membrane derived acyl chains (18:3 dominant, 18:2, 16:3 unique; e.g. Figure 1G, Supplementary Fig. S1, Supplementary Data Set 1) with infection. We further find that the unusual DGAT enzyme, the soluble AtDGAT3 metalloprotein, is localized to the chloroplast (Fig. 2C) and responsible for the bulk (60%) of powdery mildew-induced TAG synthesis in the chloroplast (Fig. 4, A and B). TLC shows TAGs from chloroplasts isolated from powdery mildew-infected leaves (Fig. 4, A and B) are enriched in TAGs that run similarly to the extra virgin olive oil standard (85% C18 and 15% C16 FAs). This suggests that the chloroplast TAGs made via AtDGAT3 are enriched for thylakoid-derived acyl chains. Furthermore, direct infusion mass spectrometry (Gutbrod et al. 2021) of lipids extracted from chloroplasts isolated from powdery mildew-infected leaves of *dgat3-2* and WT plants found TAGs comprised largely of 18:3 and 18:2 to be statistically reduced in *dgat3-2* compared with WT (Fig. 4, C and D). These findings are consistent with previous reports that AtDGAT3 preferentially incorporates C18:3, the dominant FA in thylakoid membranes, and to a lesser extent C18:2 substrates into TAGs (Hernández et al. 2012; Aymé et al. 2018). It was unclear whether AtDGAT3 could utilize C16:3 as the experimental systems employed by (Hernández et al. 2012; Aymé et al. 2018) had little available C16:3. However, we found TAG 50:6 (most likely composed of 16:0, 16:3, and 18:3) also exhibits decreased abundance in chloroplasts isolated from powdery mildew-infected *dgat3-2* compared to WT plants (Supplementary Fig. S6) suggesting this possibility.

In response to powdery mildew infection, there is a dramatic local increase in chloroplast lipid bodies (CLBs) and nearby cytoplasmic globules (CGs) (Figs. 3 and 6, Supplementary Fig. S7B). CLBs include all lipid bodies within or partly within a chloroplast and thus include plastoglobules. Chloroplast plastoglobules are lipid microcompartments associated with thylakoids that function in chloroplast metabolism, development, and response to the environment (van Wijk and Kessler 2017). We do observe some CLBs associated directly with thylakoids; however, in disintegrating chloroplasts, many CLBs are not directly associated with thylakoids though they may be of plastoglobule-origin (Fig. 6, Supplementary Fig. S7B). The electron density and size of the induced CLBs and CGs reflects those previously ascribed to plastoglobules or to be of plastoglobule-origin (Guiamét et al. 1999; Arzac et al. 2022; Bouchnak et al. 2023). DGAT3 has not been identified in Arabidopsis plastoglobule proteomics datasets (Vidi et al. 2006; Ytterberg et al. 2006; Lundquist et al. 2012; Espinoza-Corral et al. 2021); however, plastoglobule characteristics and composition are reported to vary significantly depending on stressors and developmental status (Xu et al. 2020; Arzac et al. 2022; Bouchnak et al. 2023). For example, stromal proteins have been identified in plastoglobule or plastoglobule-like subpopulations that contain thylakoid photosynthetic proteins and lipids but whose membrane varies in composition from that of thylakoid membranes (Ghosh et al. 1994; Guiamét et al. 1999; Smith et al. 2000). Furthermore, plastoglobule release into the cytosol has also been documented or implicated (Guiamét et al. 1999; Ghosh et al. 2001; Springer et al. 2016; Xu et al. 2020).

If powdery mildew-induced CLBs derive from plastoglobules, they may contain the thylakoid membrane-bound phytol ester

synthase 1 (PES1) and/or PES2 (Vidi et al. 2006; Ytterberg et al. 2006) which, in addition to phytol ester synthase activity, can synthesize TAGs via DAGs and acyl groups from acyl-CoAs (Lippold et al. 2012). As 40% of induced chloroplast TAGs remain in *dgat3-2* (Fig. 4A), it is tempting to speculate that in addition to DGAT3, PES1 and/or PES2 also contribute to powdery mildew-induced plastidic TAG synthesis.

Powdery mildew spore production is significantly reduced when AtDGAT3 expression is silenced or when null mutants in AtDGAT3 are assessed (Fig. 2B). This reduction in spore production is not associated with a pleiotropic phenotype, enhanced SA defense, and/or cell death in *dgat3-2* (Figure 4, E and F). Therefore, it appears that TAGs synthesized by DGAT3 in the chloroplast at the expense of thylakoid lipids promote powdery mildew asexual reproduction. How these TAGs directly benefit the powdery mildew remains to be determined. In response to powdery mildew-infection, leaf TAGs containing thylakoid membrane acyl chains (18:3 (dominant), 18:2, and 16:3 (unique)) accumulate (Fig. 1G, Supplementary Fig. S1B) and induced chloroplast TAGs containing 18:3, 18:2, and 16:3 are dramatically reduced in the *dgat3-2* mutant (Fig. 4, Supplementary Fig. S6). Recent evidence shows the direct transfer of lipids from plant to powdery mildew by tracking the incorporation of leaf 13C-lipid precursors to induced leaf TAGs and TAGs in newly formed PM spores that develop on the leaf (Lee et al. 2024); this includes spore TAGs containing C16:3. Using FAME, we confirm the presence of C16:3 acyl chains in spore lipids (Fig. 5C, Supplementary Data Set 3), indicative of fungal acquisition of thylakoid membrane-derived lipids. While C16:3 in spore lipids is low, it is readily detected and unlikely to reflect leaf contamination as spores are washed from infected whole leaves, filtered, spun down, and resuspended prior to lipid extraction (Methods). Instead, the low percent of 16:3 in spore lipids may reflect a preference for DGAT3 of 18:3 and 18:2 over 16:3, as well as the much lower abundance of powdery mildew-induced chloroplast TAGs with 16:3 compared with 18:3 and 18:2 (Supplementary Fig. S6, Supplementary Data Set 4). However, even though there are no annotated  $\omega$ -3 acyl lipid desaturase enzymes in the *G. orontii* MGH1 genome, we cannot exclude the possibility that *G. orontii* remodels host-acquired acyl chains to account for the 16:3 in spore TAGs using one of the uncharacterized *Gor* MGH1 fatty acid desaturases.

While TAG catabolism could serve as an immediate energy source for the fungus, these storage lipids/lipid bodies could also be transported with or without fungal remodeling to the newly developing spores which themselves are filled with lipid bodies containing TAGs (Fig. 1B). These spore storage lipids could then serve as an energy source to support spore germination and early colonization events prior to haustorium formation (Both et al. 2005). It is also possible that a host-derived lipid may be required for a fungal asexual reproductive signal. For example, in *Aspergillus nidulans* specific endogenous 18:2-derived oxylipins control sporulation versus sexual reproduction (Tsitsigiannis et al. 2004). In the arbuscular mycorrhizal fungi (AMF)—plant host symbiosis, plant-derived C16:0 2-MGs are remodeled by the AMF fungus and act both as energy sources (immediate and stored as lipid bodies in spores) and as signals for fungal development, including sporulation (Kameoka et al. 2019). For *G. orontii*, the availability of host lipid precursors dictates the number of conidiophores initiated, but not their subsequent development, suggesting host lipids or modified lipids also act as a sporulation signal (Lee et al. 2024). Plastoglobules often contain plant enzymes involved in oxylipin synthesis that could participate in the production of a fungal reproductive signal (Michel et al. 2021).

This could be particularly important for obligate biotrophs such as powdery mildews characterized by missing or incomplete pathways for specialized metabolites as compared to other *Ascomycetes* including *A. nidulans* (Spanu 2012).

## ER-associated TAGs hinder powdery mildew asexual reproduction

As shown in Fig. 7, we found mutants that limit TAG accumulation in the ER exhibit increased powdery mildew spore production (Fig. 2A), showing that opposing phenotypes are attributed to distinct TAG biosynthetic pathways. In *Arabidopsis*, DGAT1 is responsible for generating TAG from a rapidly produced pool of DAG derived from PC (Regmi et al. 2020). On the other hand, PDAT1 and DGAT2 are reported to use a different and larger pool of DAG, which has a relatively slower turnover (Regmi et al. 2020). Reduced DGAT1 expression results in ~1.5-fold enhanced spore production (Fig. 2A), while no difference is observed when PDAT1 or DGAT2 expression is perturbed (Fig. 2, A and B). This suggests a rapidly produced pool of DAG from PC available to DGAT1 is used for powdery mildew-induced TAG production in the ER (Fig. 7). Mutants in ABCA9, demonstrated to import FA/acyl-CoA into the ER, also support ~1.5-fold increased powdery mildew spore production (Fig. 2A). While LACS proteins are required for activation of imported long chain fatty acids in the ER, mutants in LACS1 (Fig. 2A) or LACS2 (Tang et al. 2007) exhibited no difference in powdery mildew asexual reproduction, likely due to functional redundancy with other ER-localized LACS proteins [LACS1, LACS2, LACS4, LACS8 (Weng et al. 2010; Zhao et al. 2010; Jessen et al. 2015)]. Collectively, our findings indicate induced TAG biosynthesis in the ER via DGAT1 impedes the asexual reproduction of powdery mildew (Fig. 7). AtDGAT1 acyl specificity differs from that of AtDGAT3. C16:0 is the preferred substrate of AtDGAT1, with little activity with C18:2 or C18:3 (Zhou et al. 2013; Aymé et al. 2014). C16:0 is a minor component of thylakoid membrane galactolipids (Browse et al. 1989; Mats et al. 2001), consistent with AtDGAT1 use of precursor pools in the ER distinct from those used in the chloroplast by AtDGAT3.

How do ER-synthesized TAGs limit the growth of the biotrophic pathogen? TAGs synthesized at the ER membrane are typically packaged into organelles known as lipid droplets (LDs) that bud from the ER and accumulate in the cytosol (Guzha et al. 2023). Sequestration of these TAGs could be a means of nutrient restriction by the host if these LDs are not accessible to the powdery mildew. Furthermore, given DGAT3-dependent TAG synthesis in the chloroplast supports powdery mildew spore production, it is likely the competing pathway for TAG synthesis in the ER via DGAT1 may divert precursors from the chloroplast pathway (Fig. 7). For example, substrates for plastidic TAG synthesis may be limited by DGAT1 activity pulling plastidic FAs to the ER and/or reducing export of DAG/DAG precursors from the ER to the chloroplast. This competition has been observed in engineered tobacco (*Nicotiana tabacum*) leaves that accumulate oil at 15% of dry weight (Zhou et al. 2020) and reflects that TAG synthesis drives precursor flux (Bates and Browse 2012).

In addition, LDs not only contain TAGs and sterol esters but may be sites of specialized biochemistry during stress (Shimada et al. 2018). Increased LDs have been observed in leaves infected by the hemi-biotrophic fungus *Colletotrichum higginsianum* and proposed to be sites of phytoalexin synthesis, preventing pathogen spread (Shimada et al. 2014). Furthermore, LDs induced in response to avirulent *Pseudomonas syringae* infection of *Arabidopsis* leaves were found to contain camalexin biosynthetic enzymes

(Fernández-Santos et al. 2020). Genes involved in indole-3-acetaldoxime-derived phytoalexin production associated with defense against powdery mildews (Clay et al. 2009; Liu et al. 2016; Hunziker et al. 2020) exhibit enhanced expression at the powdery mildew infection site at 5 dpi (Chandran et al. 2010). This raises the possibility that increased synthesis and/or exposure to defensive specialized metabolites may contribute to the reduction in powdery mildew spore production associated with ER-derived LDs (Fig. 7).

## Powdery mildew infection offers valuable insights into the intricacy of plant lipid metabolism

Although TAGs typically do not accumulate to significant levels in vegetative tissues, TAG accumulation in leaf tissue occurs in response to diverse environmental stresses and leaf senescence (Lu et al. 2020). While a role for AtDGAT3 has not been assessed in response to environmental stresses or leaf senescence, our study shows the important role AtDGAT3 plays in the powdery mildew-host interaction. This indicates that AtDGAT3 function should be examined under other conditions, particularly those in which thylakoid disassembly is observed and induced TAGs are enriched in thylakoid-derived FAs, such as senescence, heat stress, and response to N limitation (Kaup et al. 2002; Gaude et al. 2007; Besagni and Kessler 2013; Higashi et al. 2015). Furthermore, similar to our findings (Fig. 6), induced CLBs, and CGs have been observed under these conditions (Guamét et al. 1999; Zhang et al. 2010). This argues for the tracking of cytosolic LD origins in photosynthetic tissue that have often been assumed to be ER-derived. However, the powdery mildew system provides a phenotype (impact on spore production) for distinguishing chloroplast-derived TAGs (via AtDGAT3) from those produced in the ER via AtDGAT1. Whether this translates to other (obligate) plant biotrophs of vegetative tissue remains to be investigated.

As shown by the root colonizing-obligate symbiont AMF, TAGs are only one possible source of lipids for microbial acquisition. AMF manipulate plant root cells to produce 2-MGs for fungal acquisition (Kameoka and Gutjahr 2022). In both systems, localized endoreduplication occurs and is associated with enhanced metabolic capacity that may allow for increased flux to FAs (Wildermuth 2010, 2017). While AMF shifts lipid metabolism to 2-MG production through the use of enzymes specific to AMF host plants, the powdery mildew employs DGAT3, present in almost all land plants (Yan et al. 2018), for chloroplast TAG formation to support asexual reproduction (Figs. 2 and 4). Therefore, specific host transporters may not be required as they are for AMF 2-MGs. Instead, lipid bodies that originate in the chloroplast have the potential to be directly acquired by the powdery mildew. Similarly, a number of human intracellular pathogens acquire host lipid bodies for their nutrition and development (Vallochi et al. 2018).

## DGAT3, a unique class of DGAT enzyme

The 3 classes of *Arabidopsis* DGAT enzymes contain distinct conserved domains and have evolved independently in eukaryotes, with DGAT3 unique to Viridiplantae (Turchetto-Zolet et al. 2011; Yin et al. 2022). The least studied DGAT class, DGAT3 enzymes, are unique in that they are soluble metalloproteins, with no trans-membrane domain, and a thioredoxin-like ferredoxin domain containing a [2Fe-2S] cluster (Aymé et al. 2018). While AtDGAT3 (Fig. 2C) and *Paeonia rockii* PrDGAT3 (Han et al. 2022) are clearly localized to the chloroplast; other DGAT3 enzymes have been

characterized as cytosolic [peanut, (Saha et al. 2006); soybean, (Xue et al. 2022); *Camelina sativa* (Gao et al. 2021)].

AtDGAT3 is widely expressed at levels often 10-fold higher than AtDGAT1 and AtDGAT2, with highest expression in the hypocotyl and mature and senescent leaf petioles and stems (Klepikova et al. 2016). Consistent with findings for powdery mildew infection of mature *Arabidopsis* leaves (Chandran et al. 2009, 2010), AtDGAT3 is not strongly induced in response to pathogen or abiotic stress, assessed using the *Arabidopsis* eFP Browser (Winter et al. 2007). As changes in AtDGAT3 expression are minimal, AtDGAT3 activity may depend on the availability of preferred precursors (e.g. released from thylakoid degradation). Furthermore, AtDGAT3 activity may be regulated by insertion of preformed [2Fe-2S] into the apo-protein in the plastid (Przybyla-Toscano et al. 2018) and by redox (Hernández and Cejudo 2021; Hoh et al. 2024) as the oxidized form of AtDGAT3, AtDGAT3 [2Fe-2S]<sub>2</sub><sup>+</sup> cluster is stable, while the reduced [2Fe-2S]<sub>1</sub><sup>+</sup> form of the enzyme is rapidly destroyed (Aymé et al. 2018).

Engineered plants with increased TAG yield and low input costs for biofuel or specialized chemical applications (Pfleger et al. 2015) could be designed to take advantage of AtDGAT3's production of TAGs at the expense of thylakoid membranes. The associated TAG profile would be enriched in C18:3 and C18:2 fatty acids desirable for human nutrition (Kumar et al. 2016). As shown in Fig. 4, the TAGs from isolated chloroplasts infected with powdery mildew appear similar to that of commercial extra virgin olive oil and to be largely attributed to synthesis via AtDGAT3. By contrast the TAGs from infected whole leaves are dominated by TAGs with reduced FA chain length, indicated by the lower Rf, that are likely synthesized in the ER via DGAT1, consistent with its preference for C16:0 (Aymé et al. 2014). Transient expression of AtDGAT3 or PrDGAT3 in *N. benthamiana* leaves increases TAG production by ~2-fold (Hernández et al. 2012; Han et al. 2022), compared with 7- to 8-fold increase with AtDGAT1 transient expression (Hernández et al. 2012; Vanhercke et al. 2013). Therefore, in engineered plants, increased flux to plastidic TAG synthesis might be further enhanced by reducing DGAT1. In addition, controls over DGAT3 activity and stability would need to be addressed.

Not only does the powdery mildew system allow us to uncover the role of AtDGAT3 in plastid TAG biosynthesis but it can also be used to dissect key regulators driving flux towards plastid TAG synthesis and CLB secretion. While the powdery mildew-induced shift in leaf lipid metabolism is highly localized, heavy infection could further increase induced TAG levels from the 3.5-fold induction observed with the low/moderate levels of infection that facilitate our molecular and microscopic studies. By understanding how mature photosynthetically active leaves switch their metabolism to break down thylakoids to make and secrete storage lipids, higher yields of plant oils could potentially be achieved, than from extracted seeds or fruit. Furthermore, plants suitable for oil production could be expanded and deforestation associated with palm oil plantations could potentially be reduced, facilitating more sustainable and environmentally benign production.

## Materials and methods

### Plant lines, growth, and powdery mildew infection

Mutant list: Seeds of *abca9-1* [SALK\_058070 (Kim et al. 2013)], *abca9-3* [SALK\_084342 (Kim et al. 2013)], *lacs1-1* [SALK\_127191 (Lü et al. 2009)], *dgat1-1* [CS3861 or AS11 (Katavic et al. 1995)], *dgat2-1* [SALK\_067809 (Zhang et al. 2009)], *dgat3-2* (SALK\_112303, Supplementary Fig. S3), *pdat1-2* [SALK\_065334 (Zhang et al.

2009)] mutant lines in Columbia-0 (Col-0) background were obtained from Arabidopsis Biological Resource Center (ABRC) at The Ohio State University. Seeds of *dgat1-2* mutant line (ABX45) in Wassilewskija (WS) background (Routaboul et al. 1999) and wild type WS were obtained from Prof. Loïc Lepiniec at French National Institute for Agriculture, Food, and Environment (INRAE). CRISPR/Cas9-induced mutant alleles *dgat3-3.1* and *dgat3-3.2* were generated in this study following the method by Tsutsui and Higashiyama (2016; Supplementary Fig. S3). Briefly, a single guide RNA sequence targeting DGAT3 designed via CRISPR-P 2.0 (Liu et al. 2017), was cloned into the pKI1.1R vector described in Tsutsui and Higashiyama (2016). The resulting construct was transformed into wild type Col-0 plants via *A. tumefaciens* GV3101 by the floral dip method (Clough and Bent 1998). CRISPR/Cas9-induced mutants were confirmed by sequencing. Cas9-free plants homozygous of the T3 generation were used for further analysis. All lines were genotyped to confirm homozygosity, using primers in Supplementary Table S1.

Wild-type *A. thaliana* and mutants were grown in SS Metromix 200 soil (Sun Gro, Bellevue, WA, USA) in growth chambers at 22 °C with 12 h light/dark cycle, 70% relative humidity and PAR of ~120  $\mu\text{mol m}^{-2} \text{s}^{-1}$ . After stratification at 4 °C, alternating Col-0 and mutant seeds were planted in 16.5 cm insert boxes (12 plants/box; 6 boxes/flat). For whole plant spore count phenotyping, paired boxes of WT and mutant plants were inoculated at 4 weeks by settling tower with a moderate dose of 10–14 dpi conidia from *G. orontii* MGH1 at consistent time of day (Reuber et al. 1998). Leaves 7–9 were used in all analyses unless otherwise specified.

### Spray-induced gene silencing (SIGS)

SIGS protocol was adapted from McRae et al. (2023) for use in silencing *Arabidopsis* target DGAT3. pssRNAit (Ahmed et al. 2020) was used to design an efficient and specific dsRNA for DGAT3 (AT1G48300). As shown in Supplementary Fig. S2, the designed dsRNA was specific to the DGAT3 transcript with no potential 21 nt siRNAs that could efficiently cleave the DGAT1 or DGAT2 transcript. Templates were amplified (primers in Supplementary Table S1) from Col-0 cDNA and prepared for in vitro transcription with the HiScribe T7 High Yield RNA Synthesis Kit (New England Biolabs, Ipswich, MA, USA). After purification with Monarch RNA Cleanup Kit (New England Biolabs, Ipswich, MA, USA), RNA was reannealed, quantified and aliquoted in nuclease-free water. 12–15 mature fully expanded *Arabidopsis* leaves from 4 to 5 4-week-old plants were harvested. Petioles were inserted through a Whatman 1.0 paper overlaid into 1/2 mS salts (Research Products International, Prospect, IL, USA), 0.1% 2-(N-morpholino)ethanesulfonic acid (Merck Millipore, Burlington, MA, USA), and 0.8% agar (BD Biosciences, San Jose, CA, USA) in 150 mm plates. Paired plates (with mutant and WT leaves) were placed under the settling tower and infected with 10–14 dpi conidia, as above. 40  $\mu\text{g}$  RNA (or nuclease-free mock) was sprayed at 1 hpi and 2 dpi.

### Spore tissue collection and counting

Powdery mildew spore production/mg leaf fresh weight protocol was adapted from Weßling and Panstruga (Weßling and Panstruga 2012). Briefly, at 8–10 dpi, for each replicate, about 12 leaves at leaf stages 7–9 pooled from 4 or 5 WT plants or parallelly infected mutant plants, or from mock or dsRNA-treated plates, were harvested. Spores were washed off leaves by vortexing in 15 mL 0.01% Tween-80 for 30 s and filtered through 30  $\mu\text{m}$  CellTrics filter (Sysmex America, Lincolnshire, IL, USA) before centrifugation at 4000  $\times g$ . The resulting spore pellet was resuspended

in 200–1000  $\mu\text{L}$  water. For each sample, 9  $1\times 1$  mm fields of a Neubauer-improved haemocytometer were counted. For spore counting for each replicate, 3 paired counts of WT and mutant spore suspensions from a box were performed on a Neubauer-improved haemocytometer (Hausser Scientific, Horsham, PA, USA). Spore counts were divided by the fresh weight of the plant tissue to determine spores/mgFW and then normalized to WT or mock counts. To determine significance, a 2-tailed One-sample t-test was performed on counts from at least 5 boxes ( $P < 0.05$ ).

### Trypan blue staining

To visualize cell death, leaf tissues were incubated for 16 h at 24 °C in the staining solution [2.5 mg/mL trypan blue in lactophenol, lactic acid, glycerol, phenol, water (1:1:1:1)], and 2 volumes of ethanol were added to this solution. The tissues were cleared in chloral hydrate solution (2.5 g/mL chloral hydrate in water) for 16 h at 24 °C. Leaf tissues were transferred to 70% glycerol and viewed using the AS Laser Microdissection system microscope (Leica Microsystems, Deerfield, IL, USA). Note that trypan blue also slightly stains fungal structures.

### Reverse transcription (RT)-qPCR analysis

Total RNA from leaves was extracted with RNA using Spectrum (Sigma-Aldrich) Plant Total RNA Kit according to the manufacturer's protocol. Residual genomic DNA was digested with DNase I (DNaseI, Qiagen). qPCR was performed using cDNA using High-Capacity cDNA Reverse Transcription Kit (ThermoFisher Scientific). The gene specific primers for DGAT3 are: P1: 5'-ACCAGAACGGTAGGGTTTCG-3'; P2: 5'-CTAACGTTTGGCCATCAGC-3'. Amplification was performed using the following conditions: 95 °C for 2 min and 30 cycles of 95 °C for 30 s, 60 °C for 30 s, and 72 °C for 90 s.

To analyze the expression levels of genes, 3 independently grown biological replicates of two fully expanded leaves (leaves 7–9) at 5 dpi were used for comparison. Tissue was immediately frozen in liquid nitrogen and stored at  $-80$  °C until extraction. RNA was extracted using Spectrum (Sigma-Aldrich) Plant Total RNA Kit according to the manufacturer's protocol. Residual genomic DNA was digested with DNase I (DNaseI, Qiagen). Purity and concentration of RNA was confirmed with Nanodrop-1000 spectrophotometer (ThermoFisher Scientific). Complementary DNA (cDNA) was synthesized from 1  $\mu\text{g}$  RNA using High-Capacity cDNA Reverse Transcription Kit (ThermoFisher Scientific). Quantitative real-time PCR (qPCR) experiments were performed in a BioRad CFX96 (BioRad) using the iTaq Universal SYBR Green Supermix (Bio-Rad, USA), following kit instructions. For all genes, thermal cycling started with a 95 °C denaturation step for 10 min followed by 40 cycles of denaturation at 95 °C for 15 s and annealing at 56 °C for 30 s. Each run was finished with melt curve analysis to confirm specificity of amplicon. Three technical replicates were performed for each experimental set. Gene expression (fold change) was calculated normalized to ACTIN2 (At3g18780) as reference gene, and calculated using the Do My qPCR Calculations webtool ([http://umrh-bioinfo.clermont.inrae.fr/do\\_my\\_qPCRcalc/](http://umrh-bioinfo.clermont.inrae.fr/do_my_qPCRcalc/); Tournayre et al. 2019). Primer sequences are provided in Supplementary Table S1.

### Golden gate cloning and transient expression of DGAT3 via Agrobacterium infiltration

The full-length genomic DNA encoding DGAT3 (AT1G48300) without stop codon and with removal of an internal restriction site for BsaI was utilized. Two BsaI restriction enzyme sites are added to

both 5' and 3' end of sequence using PCR primers listed in Supplementary Table S1. The sequence was cloned into the pICSL22010 plasmid (with C-terminal GFP and CaMV 35S promoter) by Golden Gate cloning (Supplementary Fig. S3C). The vector was transformed into *A. tumefaciens* GV3101. *A. tumefaciens* transformants were grown in 5 mL liquid LB with appropriate antibiotics overnight at 28 °C, pelleted, resuspended in induction media (10 mM MES pH 5.6, 10 mM MgCl<sub>2</sub>, 150  $\mu\text{M}$  acetosyringone) to an OD<sub>600</sub> of 0.4–0.60 for transient expression, and incubated in induction media for approximately 3–4 h before infiltration in *N. benthamiana* leaves. GFP fluorescence was observed at 48–72 hpi by Zeiss LSM710 confocal microscope (Carl Zeiss Inc, White Plains, NY, USA) at the RCNR Biological Imaging Facility, UC Berkeley. The 35S::GFP was used as negative control. Three independent infiltrations were done. The total number of cells observed is 20 and all 20 cells showed the same localization.

### Confocal imaging

Confocal scanning fluorescence microscopy with a Zeiss LSM710 confocal microscope (Carl Zeiss Inc, White Plains, New York) at the RCNR Biological Imaging Facility, UC Berkeley was utilized to examine fungal haustoria and lipid bodies.

Col-0 lines expressing RPW8.2-YFP under the native promoter were inoculated with *G. orontii* to visualize fungal haustoria (Wang et al. 2009). The 3D reconstruction of RPW8.2-YFP was performed using Imaris software. To visualize lipid bodies, tissues were stained with 0.004 mg/mL BODIPY 505/515 and vacuum infiltrated for 10 min before imaging. Excitation of chlorophyll and BODIPY were at 633 and 488 nm, respectively. Emission wavelength for chlorophyll and BODIPY-stained lipid bodies was 647–721 nm and 493–589 nm, respectively. Percent-area of BODIPY fluorescence was quantified using Image J software. The 3D reconstruction of lipid droplets and chloroplasts was performed using Imaris.

### Transmission electron microscopy imaging

Arabidopsis Col-0 4-week-old plants were heavily inoculated with *G. orontii* or remained uninfected. Three leaves (7–9) were sampled at 5 dpi from infected or parallel uninoculated plants and cut into  $2\times 3$ -mm sections, fixed in buffer containing 2.5% glutaraldehyde, 2% tween 20, 0.05 M sodium cacodylate and 4% formaldehyde in microwave for 2 $\times$ 40 s. The fixed tissues were vacuumed for 1 h or as long as possible until they sank to the bottom. The tissues were rinsed three times in 0.05 M sodium cacodylate buffer for 10 min. After being transferred into 1% Osmium tetroxide buffer, the tissues were fixed by microwaving for 3 $\times$ 1 min, with 15 min vacuum between each microwaving. The samples were dehydrated with a gradient of acetone (35%, 50%, 70%, 80%, 95%, 100%, 100%, 100%) for 10 min each. The tissues were sequentially infiltrated with 20%, 40%, 60% resin by microwaving (3 min) and rotated overhead for 1 h after each microwaving. The samples were rotated in 80% resin for 16 h. The next day, the samples were rotated in 90% resin 16 h. The samples were embedded in a flat embedding mold and cured in a 60 °C oven for 2–3 days. Ultrathin sections were put on mesh nickel grids. After contrast staining, samples were examined and images were acquired with a FEI Tecnai T12 Transmission Electron Microscope at the UC Berkeley Electron Microscopy Laboratory. Two independent experiments were performed. TEM images looked similar, and data were combined for analyses. In Experiment 1, 5 slices contained a haustorium and in Experiment 2, 1 slice contained a haustorium. In each slice containing a haustorium, 1 to 3

mesophyll cells right underneath the haustorium were captured, with those mesophyll cells containing 3 to 15 chloroplasts captured in the same slice by TEM. In total, 8 mesophyll cells underlying a haustorium-containing epidermal cell were analyzed. Chloroplast-associated cytoplasmic globules are defined to be electron dense particles outside the chloroplast outer membrane (Guamét et al. 1999). The mean number of CGs per chloroplast was calculated for these 8 mesophyll cells. The same principle was used for counting the number of starch granules per chloroplast in each cell.

## TAGs and phospholipids via LC-MS/MS

Leaf tissue (leaves 7–9) was harvested at 12 dpi, rapidly weighed, and flash frozen until ready for extraction. Uninfected (non-inoculated) leaf tissue is collected from leaves 7–9 of uninfected plants grown in parallel. After tissue disruption in the bead beater, modified Bligh & Dyer extraction with methanol:chloroform:H<sub>2</sub>O (1:1:0.9) was performed, 300  $\mu$ L of chloroform phase was recovered, and dried under nitrogen. The dried extracts were re-suspended in 200  $\mu$ L of Isopropanol (IPA):Acetonitrile (ACN):Methanol (MeOH) (3:3:4), and run immediately. Internal standard mixes were used to ensure retention time reproducibility. Samples were run on an Agilent 1290 (Agilent Technologies, Santa Clara, CA, USA) UHPLC connected to a QExactive mass spectrometer (Thermo Fisher Scientific, San Jose, CA, USA) at the DOE Lawrence Berkeley Lab with the following chromatographic method, in both positive and negative mode. Source settings on the MS included auxiliary gas flow of 20 (au), sheath gas flow rate of 55 (au), sweep gas flow of 2 (au), spray voltage of 3 kV (positive and negative ionization modes), and ion transfer tube temperature of 400 °C.

Lipids were run on a reversed phase 50 mm  $\times$  2.1 mm, 1.8  $\mu$ m Zorbax RRHD (Rapid Resolution High Definition) C18 column (Agilent Technologies) with a 21 min gradient and 0.4 mL/min flow rate, with 2  $\mu$ L injections. The mobile phases used were A: 60:40 H<sub>2</sub>O:ACN (60:40) with 5 mM ammonium acetate, 0.1% formic acid, and B: IPA:ACN (90:10) with 5 mM ammonium acetate (0.2% H<sub>2</sub>O), 0.1% formic acid. The system was held at 20% B for 1.5 min, followed by an increase to 55% B over 2.5 min, and a subsequent increase to 80% B over 6 min. The system was then held at 80% B for 2 min, before being flushed out with 100% B for 5 min, and re-equilibrated at 20% B over 5 min. The QExactive parameters were as follows: MS resolution was set to 70,000, and data were collected in centroid mode from 80–1200 m/z. MS/MS data was collected at a resolution of 17,500 with a collision energy step gradient of 10, 20, and 30. Lipids were identified by comparing detected vs. theoretical lipid m/z and MS/MS fragmentation patterns, with lipid class and fatty acid composition determined based on characteristic product ions or neutral losses (see [Supplementary Data Set 1](#)). TAGs were detected in positive ionization mode as [M+NH<sub>4</sub>]<sup>+</sup> adducts, with FA tails determined by neutral loss of ions detected in MS/MS fragmentation spectra. Phospholipids PC, lysoPC, PE, PI, and PG were detected in positive ionization mode as [M+H]<sup>+</sup> adducts, with PCs and lysoPCs having a characteristic product ion of 184, PEs a neutral loss of 141, PIs a neutral loss of 260 and PGs a neutral loss of 172 (Murphy 2014). Metabolomics raw data are deposited in the MassIVE data repository (<https://massive.ucsd.edu/>), accession number MSV000093317 (doi: <https://doi.org/10.25345/C5N873941>). Only lipid classes that have peak heights above the upper bound of the 95% confidence interval of the negative controls are included in [Supplementary Data Set 1](#) for further analysis.

## Thylakoid membrane lipid analysis

### Tissue harvest and lipid extraction

Leaves 7–9 were harvested from uninfected and infected plants grown in parallel, washed of spores, frozen in liquid nitrogen, and stored at –80 °C until extraction. Extraction was performed following lipase inactivation in 75 °C isopropanol for 15 min according to (Devaiah et al. 2006) and electrospray ionization tandem mass spectrometry was performed at the Kansas Lipidomics Research Center Analytical Laboratory (Manhattan, KS) as below.

### Electrospray ionization tandem mass spectrometry conditions

The samples were dissolved in 1 mL chloroform. An aliquot of 10 to 20  $\mu$ L of extract in chloroform was used. Precise amounts of internal standards, obtained and quantified as previously described (Welti et al. 2002), were added in the following quantities (with some small variation in amounts in different batches of internal standards): 0.36 nmol di14:0-PG, 0.36 nmol di24:1-PG, 0.36 nmol 14:0-lysoPG, 0.36 nmol 18:0-lysoPG, 2.01 nmol 16:0–18:0-MGDG, 0.39 nmol di18:0-MGDG, 0.49 nmol 16:0–18:0-DGDG, and 0.71 nmol di18:0-DGDG. Samples were combined with solvents, introduced by continuous infusion into the ESI source on a triple quadrupole MS/MS (API 4000, Applied Biosystems, Foster City, CA), and neutral loss scans were acquired as described by (Shiva et al. 2013).

The background of each spectrum was subtracted, the data were smoothed, and peak areas integrated using a custom script and Applied Biosystems Analyst software. Peaks corresponding to the target lipids in these spectra were identified and the intensities corrected for isotopic overlap. Lipids in each class were quantified in comparison to the two internal standards of that class. The first and typically every 11th set of mass spectra were acquired on the internal standard mixture only. A correction for the reduced response of the mass spectrometer to the galactolipid standards in comparison to its response to the unsaturated leaf galactolipids was applied. To correct for chemical or instrumental noise in the samples, the molar amount of each lipid metabolite detected in the “internal standards only” spectra was subtracted from the molar amount of each metabolite calculated in each set of sample spectra. Finally, the data were corrected for the fraction of the sample analyzed and normalized to the sample leaf dry weight (DW) to produce data in the units nmol/mg DW.

### FAME analysis

Leaves 7–9 were harvested from uninfected and infected plants grown in parallel, washed of spores, frozen in liquid nitrogen, and stored at –80 °C until extraction. Extraction was performed following lipase inactivation in 75 °C isopropanol for 15 min according to (Devaiah et al. 2006) and FAME analysis was performed by the Kansas Lipidomics Research Center Analytical Laboratory (Manhattan, KS, USA) as below.

Total lipid extracts were spiked with 25 nmol pentadecanoic (C15:0) acid as internal standard. Samples were evaporated under a stream of nitrogen. Samples were resuspended in 1 mL 3 M methanolic hydrochloric acid and heated at 78 °C for 30 min. Two mL H<sub>2</sub>O and 2 mL hexane were added followed by three hexane extractions and then dried down under a stream of nitrogen. Samples were then redissolved in 100  $\mu$ L hexane and analyzed on GC-FID (Agilent 6890N) after separating sample using a DB-23 capillary column (column length, 60 m; internal diameter, 250  $\mu$ m; film thickness, 0.25  $\mu$ m). The carrier was helium gas at a

flow rate of 1.5 mL/min. The back inlet was operating at a pressure of 36.01 psi and temperature of 250 °C. The GC oven temperature ramp began with an initial temperature of 150 °C held for 1 min and increased at 25 °C/min to 175 °C. Then the temperature was increased at 4 °C/min to 230 °C and held at 230 °C for 8 min. The total run time was 23.75 min. The flame ionization detector was operated at 260 °C. The hydrogen flow to the detector was 30 mL/min, air flow was 400 mL/min and sampling rate of the FID was 20 Hz. The data were processed using Agilent Chemstation software. As for above, only data with CoV < 0.3 were included. Data are presented as nmol/mg DW of the tissue utilized. Spore nmol/mg DW was multiplied by 0.12995 to indicate the corresponding leaf mg/DW from which the spores were obtained.

## Lipid extraction and analysis for TLC and direct infusion mass spectrometry

Chloroplast isolation: leaf tissue, pooled from about 40 *Arabidopsis* plants per sample infected with *G. orontii* MGH1 at 4 weeks, was harvested at 12 dpi or from uninfected plants of the same age grown in parallel, and immediately homogenized by blending for 3 × 5 s in isolation buffer (30 mM HEPES-KOH pH 8, 0.33 M sorbitol, 5 mM MgCl<sub>2</sub>, 0.1% [w/v] BSA). The resulting homogenate was briefly filtered through one layer of Mira cloth (Chicopee Mills Inc., Milltown, NJ, USA). Chloroplasts were pelleted with 5-min centrifugation at 1500 g and 4 °C and washed twice with washing buffer (30 mM HEPES-KOH pH 8.0, 0.33 M sorbitol). Washed chloroplasts were normalized by chlorophyll concentration and resuspended in an osmotic stress buffer (10 mM Tricine pH 7.9, 1 mM EDTA, 0.6 M sucrose) and stored at -80 °C for future analysis.

Lipid extraction and analysis for TLC: 1–3 mg chloroplasts (normalized by chlorophyll concentrations) or 1–2 g grounded whole leaf tissues pooled from 4- to 5-week-old plants (normalized by fresh weight) for infected samples at 12 dpi were sonicated with 4 pulses of 10 s and 20% wattage (Model VCX 130, Sonics & Materials INC, Newtown, CT, USA). One milliliter of 2:1 Chloroform Methanol (v/v) with 0.01%BHT was added and placed on a vortex for 5 min. Two hundred sixty-six microliters of 0.73% (w/v) NaCl solution was added, and the mixture was inverted 5–6 times to mix. Samples were then centrifuged for 5 min at 10,000 × g. The lower, solvent phase was used and dried under an N<sub>2</sub> stream and resuspended in 20 μL chloroform. In total, 10 μL of the concentrated lipid extract was loaded onto a clean silica TLC plate (MilliporeSigma TLC Silica Gel 60 F254: 25 Glass plates, M1057150001) and developed hexane:diethyl ether:glacial acetic acid (91:39:1.3) for 30 min. Lipids were visualized by sulfuric acid spray and charring (25% H<sub>2</sub>SO<sub>4</sub> in 50% ethanol, 135 °C for 10 min). Trader Giotto's extra virgin olive oil (0.01 μg loaded) was used as a standard. TLC was conducted in four independent experiments, with each serving as a biological replicate. Relative TAG content analysis was performed using ImageJ software.

Lipid extraction and analysis for direct infusion mass spectrometry: ~200 μg chloroplasts from infected samples at 12 dpi were sonicated with 4 pulses of 10 s and 20% wattage (Model VCX 130, Sonics & Materials INC, Newtown, CT, USA). Lipids were extracted following Section 3 by Gutbrod *et al.* with modifications (Gutbrod *et al.* 2021). Briefly, 1 mL MTBE was added to the isolated chloroplasts. The mixed solution was vortexed and incubated for 2 min, two times. A 50 μL internal standard mix for TAGs was added, followed by 1 mL MTBE and 0.75 mL 300 mM ammonium acetate. The samples were vortexed for 30 s and centrifuged for 5 min at 1000 g for phase separation. The upper phase (green)

was transferred to a new Eppendorf tube and dried under nitrogen. Lipid fractionation via SPE and direct infusion MS/MS are as described in Gutbrod *et al.* (2021). The abundances of TAG species were normalized by chlorophyll concentration and transformed into a percent of total TAGs for a given sample. The differences in percentages of TAG species between Col-0 and *dgat3-2* were examined using unpaired, 2-tailed Student's t-test (see [Supplementary Data Set 2](#)).

## Accession numbers

ABCA9 (AT5G61730), LACS1 (AT2G47240), PDAT1 (AT5G13640), DGAT1 (AT2G19450), DGAT2 (AT3G51520), DGAT3 (AT1G48300), PR1 (At2g14610), MassIVE data repository (<https://massive.ucsd.edu/>) accession number MSV000093317.

## Acknowledgments

We thank Dr. Denise Schichnes at the RCNR Biological Imaging Facility and the staff of the Electron Microscope Laboratory at the University of California Berkeley for their assistance. The ESI-MS/MS and FAME analyses described in this work were performed at the Kansas Lipidomics Research Center Analytical Laboratory (Manhattan, KS, USA) by Mary Roth and Libin Yao. We thank Dr. Shunyuan Xiao (University of Maryland, College Park) for RPW8-YFP *Arabidopsis* seeds, Dr. Ksenia Krasileva (UC Berkeley) for plasmid pICSL22010, and Dr. Krishna Niyogi and Claudine Tahmin (UC Berkeley) for critical review of the manuscript.

## Author contributions

M.C.W. directed the research. H.X., J.J., and M.C.W. planned and designed the research. H.X. and J.J. performed molecular genetic, microscopic, plant pathology assays, and preparation of samples for downstream lipid analyses. H.X. and E.H.C. did TLC analyses. E.R.M. also performed plant pathology assays. LC-MS/MS TAG and PL analyses were done by J.S., K.L., and T.R.N. K.G. and P.D. performed the direct infusion MS TAG analyses. H.X., J.J., and M.C.W. wrote the manuscript. All authors contributed to the reviewing of the manuscript.

## Supplementary data

The following materials are available in the online version of this article.

**Supplementary Figure S1.** Abundance of TAG species detected in infected leaves at 12 dpi, compared to uninfected leaves.

**Supplementary Figure S2.** Expression of *DGAT3* in control and SIGS-treated plants.

**Supplementary Figure S3.** Identification of *dgat3-2* (SALK\_112303), CRISPR/Cas9-induced *dgat3-3.1* and *dgat3-3.2* mutants, and plasmid map of pICSL22010-DGAT3.

**Supplementary Figure S4.** BODIPY 505/515 staining of neutral lipids in the mesophyll cell layers of rosette leaves at 5 dpi.

**Supplementary Figure S5.** TAG content in infected chloroplasts is decreased in *dgat3-3.1*.

**Supplementary Figure S6.** Percentage of TAG species in *dgat3-2* vs. Col-0 chloroplast lipid extracts from leaves at 12 dpi.

**Supplementary Figure S7.** TEM image of mesophyll cell chloroplasts.

**Supplementary Table S1.** Genotyping, cloning, and SIGS dsRNA template primers used for this work.

**Supplementary Data Set 1.** Lipid LC-MS/MS analysis.

**Supplementary Data Set 2.** Direct infusion MS analysis of chloroplast triacylglycerols.

**Supplementary Data Set 3.** FAME and ESI-MS/MS lipid analyses.

**Supplementary Data Set 4.** Statistical analyses for this study.

## Funding

This work was supported by US National Science Foundation (NSF) MCB-1617020 and PFI-1919244, and USDA National Institute of Food and Agriculture (NIFA), Hatch Project Accession Number 1016994 awards to MCW. HX also received a National Restaurant Association Educational Foundation Viticulture and Enology Scholarship. JS was supported through NSF MCB-1617020, with TN as co-PI. KL acknowledges support from the US Department of Energy Joint Genome Institute (<https://ror.org/04xm1d337>; operated under Contract No. DE-AC02-05CH11231 to Lawrence Berkeley National Laboratory). Microscopy imaging reported in this publication was supported in part by the US National Institutes of Health (NIH) S10 program under award number 1S10RR026866-01. For FAME and ESI-MS/MS analyses at the Kansas Lipidomics Research Center Analytical Laboratory, instrument acquisition and lipidomics method development were supported by the NSF (including support from the Major Research Instrumentation program; most recent award DBI-1726527), K-IDeA Networks of Biomedical Research Excellence (INBRE) of NIH (P20GM103418), USDA NIFA (Hatch/Multi-State project 1013013), and Kansas State University.

*Conflict of interest statement.* None declared.

## Data availability

The data underlying this article are available in the article, in its on-line supplementary material, and in the MassIVE data repository (<https://massive.ucsd.edu/>), accession number MSV000093317 (doi:10.25345/C5N873941).

## References

- Aboud JK, Lösel DM. Effects of powdery mildew infection on the lipid metabolism of cucumber. In: Biacs PA, Gruiz K, Kremmer T, editors. *Biological role of plant lipids*. Boston, MA: Springer US; 1989. p. 597–601.
- Ahmed F, Senthil-Kumar M, Dai X, et al. pssRNAit: a web server for designing effective and specific plant siRNAs with genome-wide off-target assessment. *Plant Physiol*. 2020;184(1):65–81. <https://doi.org/10.1104/pp.20.00293>
- Arzac MI, Fernández-Marín B, García-Plazaola JI. More than just lipid balls: quantitative analysis of plastoglobule attributes and their stress-related responses. *Planta*. 2022;255(3):62. <https://doi.org/10.1007/s00425-022-03848-9>
- Atella GC, Bittencourt-Cunha PR, Nunes RD, Shahabuddin M, Silva-Neto MAC. The major insect lipoprotein is a lipid source to mosquito stages of malaria parasite. *Acta Trop*. 2009;109(2):159–162. <https://doi.org/10.1016/j.actatropica.2008.10.004>
- Aymé L, Arragain S, Canonge M, Baud S, Touati N, Bimai O, Jagic F, Louis-Mondésir C, Briozzo P, Fontecave M, et al. *Arabidopsis thaliana* DGAT3 is a [2Fe-2S] protein involved in TAG biosynthesis. *Sci Rep*. 2018;8(1):17254. <https://doi.org/10.1038/s41598-018-35545-7>
- Aymé L, Baud S, Dubreucq B, Joffre F, Chardot T. Function and localization of the *Arabidopsis thaliana* diacylglycerol acyltransferase DGAT2 expressed in yeast. *PLoS One*. 2014;9(3):e92237. <https://doi.org/10.1371/journal.pone.0092237>
- Bates PD. Chapter six—the plant lipid metabolic network for assembly of diverse triacylglycerol molecular species. In: Rébeillé F, Maréchal E, editors. *Advances in botanical research*, vol 101. Cambridge (MA): Academic Press; 2022. p. 225–252.
- Bates PD, Browse J. The significance of different diacylglycerol synthesis pathways on plant oil composition and bioengineering. *Front Plant Sci*. 2012;3:147. <https://doi.org/10.3389/fpls.2012.00147>
- Baud S, Dubreucq B, Miquel M, Rochat C, Lepiniec L. Storage reserve accumulation in *Arabidopsis*: metabolic and developmental control of seed filling. *Arabidopsis Book*. 2008;6:e0113. doi:<https://doi.org/10.1199/tab.0113>
- Besagni C, Kessler F. A mechanism implicating plastoglobules in thylakoid disassembly during senescence and nitrogen starvation. *Planta*. 2013;237(2):463–470. <https://doi.org/10.1007/s00425-012-1813-9>
- Both M, Csukai M, Stumpf MPH, Spanu PD. Gene expression profiles of *Blumeria graminis* indicate dynamic changes to primary metabolism during development of an obligate biotrophic pathogen. *Plant Cell*. 2005;17(7):2107–2122. <https://doi.org/10.1105/tpc.105.032631>
- Bouchnak I, Coulon D, Salis V, D'Andréa S, Bréhélin C. Lipid droplets are versatile organelles involved in plant development and plant response to environmental changes. *Front Plant Sci*. 2023;14:1193905. <https://doi.org/10.3389/fpls.2023.1193905>
- Browse J, Kunst L, Anderson S, Hugly S, Somerville C. A mutant of *Arabidopsis* deficient in the chloroplast 16:1/18:1 desaturase. *Plant Physiol*. 1989;90(2):522–529. <https://doi.org/10.1104/pp.90.2.522>
- Browse J, Warwick N, Somerville CR, Slack CR. Fluxes through the prokaryotic and eukaryotic pathways of lipid synthesis in the '16:3' plant *Arabidopsis thaliana*. *Biochem J*. 1986;235(1):25–31. <https://doi.org/10.1042/bj2350025>
- Cavaco AR, Matos AR, Figueiredo A. Speaking the language of lipids: the cross-talk between plants and pathogens in defence and disease. *Cell Mol Life Sci*. 2021;78(9):4399–4415. <https://doi.org/10.1007/s00018-021-03791-0>
- Chandran D, Inada N, Hather G, Kleindt CK, Wildermuth MC. Laser microdissection of *Arabidopsis* cells at the powdery mildew infection site reveals site-specific processes and regulators. *Proc Natl Acad Sci U S A*. 2010;107(1):460–465. <https://doi.org/10.1073/pnas.0912492107>
- Chandran D, Tai YC, Hather G, Dewdney J, Denoux C, Burgess DG, Ausubel FM, Speed TP, Wildermuth MC. Temporal global expression data reveal known and novel salicylate-impacted processes and regulators mediating powdery mildew growth and reproduction on *Arabidopsis*. *Plant Physiol*. 2009;149(3):1435–1451. <https://doi.org/10.1104/pp.108.132985>
- Clark JIM, Hall JL. Solute transport into healthy and powdery mildew-infected leaves of pea and uptake by powdery mildew mycelium. *New Phytol*. 1998;140(2):261–269. <https://doi.org/10.1046/j.1469-8137.1998.00263.x>
- Clay NK, Adio AM, Denoux C, Jander G, Ausubel FM. Glucosinolate metabolites required for an *Arabidopsis* innate immune response. *Science*. 2009;323(5910):95–101. <https://doi.org/10.1126/science.1164627>
- Clough SJ, Bent AF. Floral dip: a simplified method for agrobacterium-mediated transformation of *Arabidopsis thaliana*. *Plant J*. 1998;16(6):735–743. <https://doi.org/10.1046/j.1365-313x.1998.00343.x>
- Costa G, Gildenhard M, Eldering M, Lindquist RL, Hauser AE, Sauerwein R, Goosmann C, Brinkmann V, Carrillo-Bustamante P, Levashina EA. Non-competitive resource exploitation within mosquito shapes within-host malaria infectivity and virulence.

- Nat Commun. 2018;9(1):3474. <https://doi.org/10.1038/s41467-018-05893-z>
- Dahlqvist A, Ståhl U, Lenman M, Banas A, Lee M, Sandager L, Ronne H, Stymne S. Phospholipid:diacylglycerol acyltransferase: an enzyme that catalyzes the acyl-CoA-independent formation of triacylglycerol in yeast and plants. *Proc Natl Acad Sci U S A*. 2000;97(12):6487–6492. <https://doi.org/10.1073/pnas.120067297>
- Devaiah SP, Roth MR, Baughman E, Li M, Tamura P, Jeannotte R, Welti R, Wang X. Quantitative profiling of polar glycerolipid species from organs of wild-type *Arabidopsis* and a phospholipase *dalpa1* knockout mutant. *Phytochemistry*. 2006;67(17):1907–1924. <https://doi.org/10.1016/j.phytochem.2006.06.005>
- Espinoza-Corral R, Schwenkert S, Lundquist PK. Molecular changes of *Arabidopsis thaliana* plastoglobules facilitate thylakoid membrane remodeling under high light stress. *Plant J*. 2021;106(6):1571–1587. <https://doi.org/10.1111/tbj.15253>
- Fan J, Yan C, Xu C. Phospholipid:diacylglycerol acyltransferase-mediated triacylglycerol biosynthesis is crucial for protection against fatty acid-induced cell death in growing tissues of *Arabidopsis*. *Plant J*. 2013;76(6):930–942. <https://doi.org/10.1111/tbj.12343>
- Fernández-Santos R, Izquierdo Y, López A, Muñiz L, Martínez M, Cascón T, Hamberg M, Castresana C. Protein profiles of lipid droplets during the hypersensitive defense response of *Arabidopsis* against *Pseudomonas* infection. *Plant Cell Physiol*. 2020;61(6):1144–1157. <https://doi.org/10.1093/pcp/pcaa041>
- Fotopoulos V, Gilbert MJ, Pittman JK, Marvier AC, Buchanan AJ, Sauer N, Hall JL, Williams LE. The monosaccharide transporter gene, *AtSTP4*, and the cell-wall invertase, *atbetafruct1*, are induced in *Arabidopsis* during infection with the fungal biotroph *Erysiphe cichoracearum*. *Plant Physiol*. 2003;132(2):821–829. <https://doi.org/10.1104/pp.103.021428>
- Frye CA, Innes RW. An *Arabidopsis* mutant with enhanced resistance to powdery mildew. *Plant Cell*. 1998;10(6):947–956. <https://doi.org/10.1105/tpc.10.6.947>
- Frye CA, Tang D, Innes RW. Negative regulation of defense responses in plants by a conserved MAPKK kinase. *Proc Natl Acad Sci U S A*. 2001;98(1):373–378. <https://doi.org/10.1073/pnas.98.1.373>
- Gao H, Gao Y, Zhang F, Liu B, Ji C, Xue J, Yuan L, Li R. Functional characterization of a novel acyl-CoA:diacylglycerol acyltransferase 3-3 (*CsDGAT3-3*) gene from *Camelina sativa*. *Plant Sci*. 2021;303:110752. <https://doi.org/10.1016/j.plantsci.2020.110752>
- Gaude N, Bréhélin C, Tischendorf G, Kessler F, Dörmann P. Nitrogen deficiency in *Arabidopsis* affects galactolipid composition and gene expression and results in accumulation of fatty acid phytyl esters. *Plant J*. 2007;49(4):729–739. <https://doi.org/10.1111/j.1365-3113.2006.02992.x>
- Ghosh S, Hudak KA, Dumbroff EB, Thompson JE. Release of photosynthetic protein catabolites by blebbing from thylakoids. *Plant Physiol*. 1994;106(4):1547–1553. <https://doi.org/10.1104/pp.106.4.1547>
- Ghosh S, Mahoney SR, Penterman JN, Peirson D, Dumbroff EB. Ultrastructural and biochemical changes in chloroplasts during *Brassica napus* senescence. *Plant Physiol Biochem*. 2001;39(9):777–784. [https://doi.org/10.1016/S0981-9428\(01\)01296-7](https://doi.org/10.1016/S0981-9428(01)01296-7)
- Glawe DA. The powdery mildews: a review of the World's most familiar (yet poorly known) plant pathogens. *Annu Rev Phytopathol*. 2008;46(1):27–51. <https://doi.org/10.1146/annurev.phyto.46.081407.104740>
- Guimét JJ, Pichersky E, Noodén LD. Mass exodus from senescing soybean chloroplasts. *Plant Cell Physiol*. 1999;40(9):986–992. <https://doi.org/10.1093/oxfordjournals.pcp.a029632>
- Gutbrod K, Peisker H, Dörmann P. Direct infusion mass spectrometry for complex lipid analysis. *Methods Mol Biol*. 2021;2295:101–115. [https://doi.org/10.1007/978-1-0716-1362-7\\_7](https://doi.org/10.1007/978-1-0716-1362-7_7)
- Guzha A, Whitehead P, Ischebeck T, Chapman KD. Lipid droplets: packing hydrophobic molecules within the aqueous cytoplasm. *Annu Rev Plant Biol*. 2023;74(1):195–223. <https://doi.org/10.1146/annurev-arplant-070122-021752>
- Han L, Zhai Y, Wang Y, Shi X, Xu Y, Gao S, Zhang M, Luo J, Zhang Q. Diacylglycerol acyltransferase 3 (*DGAT3*) is responsible for the biosynthesis of unsaturated fatty acids in vegetative organs of *Paeonia rockii*. *Int J Mol Sci*. 2022;23(22):14390. <https://doi.org/10.3390/ijms232214390>
- Hernández ML, Cejudo FJ. Chloroplast lipids metabolism and function. A redox perspective. *Front Plant Sci*. 2021;12:712022. <https://doi.org/10.3389/fpls.2021.712022>
- Hernández ML, Whitehead L, He Z, Gazda V, Gilday A, Kozhevnikova E, Vaistij FE, Larson TR, Graham IA. A cytosolic acyltransferase contributes to triacylglycerol synthesis in sucrose-rescued *Arabidopsis* seed oil catabolism mutants. *Plant Physiol*. 2012;160(1):215–225. <https://doi.org/10.1104/pp.112.201541>
- Higashi Y, Okazaki Y, Myouga F, Shinozaki K, Saito K. Landscape of the lipidome and transcriptome under heat stress in *Arabidopsis thaliana*. *Sci Rep*. 2015;5(1):10533. <https://doi.org/10.1038/srep10533>
- Hoh D, Froehlich JE, Kramer DM. Redox regulation in chloroplast thylakoid lumen: the pmf changes everything, again. *Plant Cell Environ*. 2024;47(8):2749–2765. <https://doi.org/10.1111/pce.14789>
- Hözl G, Dörmann P. Chloroplast lipids and their biosynthesis. *Annu Rev Plant Biol*. 2019;70(1):51–81. <https://doi.org/10.1146/annurev-arplant-050718-100202>
- Hunziker P, Ghareeb H, Wagenknecht L, Crocoll C, Halkier BA, Lipka V, Schulz A. De novo indol-3-ylmethyl glucosinolate biosynthesis, and not long-distance transport, contributes to defence of *Arabidopsis* against powdery mildew. *Plant Cell Environ*. 2020;43(6):1571–1583. <https://doi.org/10.1111/pce.13766>
- Jessen D, Roth C, Wiermer M, Fulda M. Two activities of long-chain acyl-coenzyme A synthetase are involved in lipid trafficking between the endoplasmic reticulum and the plastid in *Arabidopsis*. *Plant Physiol*. 2015;167(2):351–366. <https://doi.org/10.1104/pp.114.250365>
- Jiang Y, Wang W, Xie Q, Liu N, Liu L, Wang D, Zhang X, Yang C, Chen X, Tang D, et al. Plants transfer lipids to sustain colonization by mutualistic mycorrhizal and parasitic fungi. *Science*. 2017;356(6343):1172–1175. <https://doi.org/10.1126/science.aam9970>
- Kachroo A, Kachroo P. Fatty acid—derived signals in plant defense. *Annu Rev Phytopathol*. 2009;47(1):153–176. <https://doi.org/10.1146/annurev-phyto-080508-081820>
- Kameoka H, Gutjahr C. Functions of lipids in development and reproduction of arbuscular mycorrhizal fungi. *Plant Cell Physiol*. 2022;63(10):1356–1365. <https://doi.org/10.1093/pcp/pcac113>
- Kameoka H, Maeda T, Okuma N, Kawaguchi M. Structure-specific regulation of nutrient transport and metabolism in arbuscular mycorrhizal fungi. *Plant Cell Physiol*. 2019;60(10):2272–2281. <https://doi.org/10.1093/pcp/pcz122>
- Katavic V, Reed DW, Taylor DC, Giblin EM, Barton DL, Zou J, Mackenzie SL, Covello PS, Kunst L. Alteration of seed fatty acid composition by an ethyl methanesulfonate-induced mutation in *Arabidopsis thaliana* affecting diacylglycerol acyltransferase activity. *Plant Physiol*. 1995;108(1):399–409. <https://doi.org/10.1104/pp.108.1.399>
- Kaup MT, Froese CD, Thompson JE. A role for diacylglycerol acyltransferase during leaf senescence. *Plant Physiol*. 2002;129(4):1616–1626. <https://doi.org/10.1104/pp.003087>

- Kim S, Yamaoka Y, Ono H, Kim H, Shim D, Maeshima M, Martinoia E, Cahoon EB, Nishida I, Lee Y. AtABCA9 transporter supplies fatty acids for lipid synthesis to the endoplasmic reticulum. *Proc Natl Acad Sci U S A*. 2013;110(2):773–778. <https://doi.org/10.1073/pnas.1214159110>
- Klepikova AV, Kasianov AS, Gerasimov ES, Logacheva MD, Penin AA. A high resolution map of the *Arabidopsis thaliana* developmental transcriptome based on RNA-seq profiling. *Plant J*. 2016;88(6):1058–1070. <https://doi.org/10.1111/tpj.13312>
- Koh S, André A, Edwards H, Ehrhardt D, Somerville S. *Arabidopsis thaliana* subcellular responses to compatible *Erysiphe cichoracearum* infections. *Plant J*. 2005;44(3):516–529. <https://doi.org/10.1111/j.1365-313X.2005.02545.x>
- Kumar A, Sharma A, Upadhyaya KC. Vegetable oil: nutritional and industrial perspective. *Curr Genomics*. 2016;17(3):230–240. <https://doi.org/10.2174/1389202917666160202220107>
- Lee MY, Jaenisch J, McRae AG, Hirai-Adachi C, Louie K, Silva LP, Bowen BP, Northen TR, Wildermuth MC. 2024. Altered host pyruvate metabolism fuels and regulates fungal asexual reproduction. *bioRxiv* 2024. <https://doi.org/10.1101/2024.08.22.609210>, preprint: not peer reviewed.
- Liang P, Liu S, Xu F, Jiang S, Yan J, He Q, Liu W, Lin C, Zheng F, Wang X, et al. Powdery mildews are characterized by contracted carbohydrate metabolism and diverse effectors to adapt to obligate biotrophic lifestyle. *Front Microbiol*. 2018;9:3160. <https://doi.org/10.3389/fmicb.2018.03160>
- Lippold F, vom Dorp K, Abraham M, Hölzl G, Wewer V, Yilmaz JL, Lager I, Montandon C, Besagni C, Kessler F, et al. Fatty acid phytyl ester synthesis in chloroplasts of *Arabidopsis*. *Plant Cell*. 2012;24(5):2001–2014. <https://doi.org/10.1105/tpc.112.095588>
- Liu H, Ding Y, Zhou Y, Jin W, Xie K, Chen L-L. CRISPR-P 2.0: an improved CRISPR-cas9 tool for genome editing in plants. *Mol Plant*. 2017;10(3):530–532. <https://doi.org/10.1016/j.molp.2017.01.003>
- Liu S, Bartnikas LM, Volko SM, Ausubel FM, Tang D. Mutation of the glucosinolate biosynthesis enzyme cytochrome P450 83A1 mono-oxygenase increases camalexin accumulation and powdery mildew resistance. *Front Plant Sci*. 2016;7:227. <https://doi.org/10.3389/fpls.2016.00227>
- Lu J, Xu Y, Wang J, Singer SD, Chen G. The role of triacylglycerol in plant stress response. *Plants*. 2020;9(4):472. <https://doi.org/10.3390/plants9040472>
- Lü S, Song T, Kosma DK, Parsons EP, Rowland O, Jenks MA. *Arabidopsis* CER8 encodes LONG-CHAIN ACYL-COA SYNTHETASE 1 (LACS1) that has overlapping functions with LACS2 in plant wax and cutin synthesis. *Plant J*. 2009;59(4):553–564. <https://doi.org/10.1111/j.1365-313X.2009.03892.x>
- Luginbuehl LH, Menard GN, Kurup S, Van Erp H, Radhakrishnan GV, Breakspear A, Oldroyd GED, Eastmond PJ. Fatty acids in arbuscular mycorrhizal fungi are synthesized by the host plant. *Science*. 2017;356(6343):1175–1178. <https://doi.org/10.1126/science.aan0081>
- Lundquist PK, Poliakov A, Bhuiyan NH, Zybailov B, Sun Q, van Wijk KJ. The functional network of the *Arabidopsis* plastoglobule proteome based on quantitative proteomics and genome-wide co-expression analysis. *Plant Physiol*. 2012;158(3):1172–1192. <https://doi.org/10.1104/pp.111.193144>
- MacLean AM, Bravo A, Harrison MJ. Plant signaling and metabolic pathways enabling arbuscular mycorrhizal symbiosis. *Plant Cell*. 2017;29(10):2319–2335. <https://doi.org/10.1105/tpc.17.00555>
- Mats XA, Magnus Kjellberg J, Sandelius AS. Chloroplast biogenesis. Regulation of lipid transport to the thylakoid in chloroplasts isolated from expanding and fully expanded leaves of pea. *Plant Physiol*. 2001;127(1):184–193. <https://doi.org/10.1104/pp.127.1.184>
- McRae AG, Taneja J, Yee K, Shi X, Haridas S, LaButti K, Singan V, Grigoriev IV, Wildermuth MC. Spray-induced gene silencing to identify powdery mildew gene targets and processes for powdery mildew control. *Mol Plant Pathol*. 2023;24(9):1168–1183. <https://doi.org/10.1111/mpp.13361>
- Micali C, Göllner K, Humphry M, Consonni C, Panstruga R. The powdery mildew disease of *Arabidopsis*: a paradigm for the interaction between plants and biotrophic fungi. *Arabidopsis Book*. 2008;6:e0115. <https://doi.org/10.1199/tab.0115>
- Michel EJS, Ponnala L, van Wijk KJ. Tissue-type specific accumulation of the plastoglobular proteome, transcriptional networks, and plastoglobular functions. *J Exp Bot*. 2021;72(13):4663–4679. <https://doi.org/10.1093/jxb/erab175>
- Moellering ER, Muthan B, Benning C. Freezing tolerance in plants requires lipid remodeling at the outer chloroplast membrane. *Science*. 2010;330(6001):226–228. <https://doi.org/10.1126/science.1191803>
- Murphy RC. *Tandem mass spectrometry of lipids: molecular analysis of complex lipids*. Cambridge (UK): Royal Society of Chemistry; 2014.
- Okazaki Y, Saito K. Roles of lipids as signaling molecules and mitigators during stress response in plants. *Plant J*. 2014;79(4):584–596. <https://doi.org/10.1111/tpj.12556>
- Pfleger BF, Gossing M, Nielsen J. Metabolic engineering strategies for microbial synthesis of oleochemicals. *Metab Eng*. 2015;29:1–11. <https://doi.org/10.1016/j.ymben.2015.01.009>
- Przybyla-Toscano J, Roland M, Gaymard F, Couturier J, Rouhier N. Roles and maturation of iron-sulfur proteins in plastids. *J Biol Inorg Chem*. 2018;23(4):545–566. <https://doi.org/10.1007/s00775-018-1532-1>
- Regmi A, Shockey J, Kotapati HK, Bates PD. Oil-producing metabolons containing DGAT1 use separate substrate pools from those containing DGAT2 or PDAT. *Plant Physiol*. 2020;184(2):720–737. <https://doi.org/10.1104/pp.20.00461>
- Reuber TL, Plotnikova JM, Dewdney J, Rogers EE, Wood W, Ausubel FM. Correlation of defense gene induction defects with powdery mildew susceptibility in *Arabidopsis* enhanced disease susceptibility mutants. *Plant J*. 1998;16(4):473–485. <https://doi.org/10.1046/j.1365-313x.1998.00319.x>
- Routaboul JM, Benning C, Bechtold N, Caboche M, Lepiniec L. The TAG1 locus of *Arabidopsis* encodes for a diacylglycerol acyltransferase. *Plant Physiol Biochem*. 1999;37(11):831–840. [https://doi.org/10.1016/S0981-9428\(99\)00115-1](https://doi.org/10.1016/S0981-9428(99)00115-1)
- Saha S, Enugutti B, Rajakumari S, Rajasekharan R. Cytosolic triacylglycerol biosynthetic pathway in oilseeds. Molecular cloning and expression of peanut cytosolic diacylglycerol acyltransferase. *Plant Physiol*. 2006;141(4):1533–1543. <https://doi.org/10.1104/pp.106.082198>
- Shimada TL, Hayashi M, Hara-Nishimura I. Membrane dynamics and multiple functions of oil bodies in seeds and leaves. *Plant Physiol*. 2018;176(1):199–207. <https://doi.org/10.1104/pp.17.01522>
- Shimada TL, Takano Y, Shimada T, Fujiwara M, Fukao Y, Mori M, Okazaki Y, Saito K, Sasaki R, Aoki K, et al. Leaf oil body functions as a subcellular factory for the production of a phytoalexin in *Arabidopsis*. *Plant Physiol*. 2014;164(1):105–118. <https://doi.org/10.1104/pp.113.230185>
- Shiva S, Vu HS, Roth MR, Zhou Z, Reddy Marepally S, Sagar Nune D, Lushington GH, Visvanathan M, Welti R. Lipidomic analysis of plant membrane lipids by direct infusion tandem mass spectrometry. *Methods Mol Biol*. 2013;1009:79–91. [https://doi.org/10.1007/978-1-62703-401-2\\_9](https://doi.org/10.1007/978-1-62703-401-2_9)
- Smith MD, Licatalosi DD, Thompson JE. Co-association of cytochrome F catabolites and plastid-lipid-associated protein with

- chloroplast lipid particles. *Plant Physiol.* 2000;124(1):211–222. <https://doi.org/10.1104/pp.124.1.211>
- Spanu PD. The genomics of obligate (and nonobligate) biotrophs. *Annu Rev Phytopathol.* 2012;50(1):91–109. <https://doi.org/10.1146/annurev-phyto-081211-173024>
- Springer A, Kang C, Rustgi S, von Wettstein D, Reinbothe C, Pollmann S, Reinbothe S. Programmed chloroplast destruction during leaf senescence involves 13-lipoxygenase (13-LOX). *Proc Natl Acad Sci U S A.* 2016;113(12):3383–3388. <https://doi.org/10.1073/pnas.1525747113>
- Sutton PN, Henry MJ, Hall JL. Glucose, and not sucrose, is transported from wheat to wheat powdery mildew. *Planta.* 1999;208(3):426–430. <https://doi.org/10.1007/s004250050578>
- Swarbrick PJ, Schulze-Lefert P, Scholes JD. Metabolic consequences of susceptibility and resistance (race-specific and broad-spectrum) in barley leaves challenged with powdery mildew. *Plant Cell Environ.* 2006;29(6):1061–1076. <https://doi.org/10.1111/j.1365-3040.2005.01472.x>
- Tang D, Simonich MT, Innes RW. Mutations in LACS2, a long-chain acyl-coenzyme A synthetase, enhance susceptibility to avirulent *Pseudomonas syringae* but confer resistance to *Botrytis cinerea* in *Arabidopsis*. *Plant Physiol.* 2007;144(2):1093–1103. <https://doi.org/10.1104/pp.106.094318>
- Tournayre J, Reichstadt M, Parry L, Fafournoux P, Jousse C. ‘Do My qPCR Calculation’, a web tool. *Bioinformatics.* 2019;15(5):369–372. <https://doi.org/10.6026/97320630015369>
- Tsitsigiannis DI, Kowieski TM, Zarnowski R, Keller NP. Endogenous lipogenic regulators of spore balance in *Aspergillus nidulans*. *Eukaryot Cell.* 2004;3(6):1398–1411. <https://doi.org/10.1128/EC.3.6.1398-1411.2004>
- Tsutsui H, Higashiyama T. pKAMA-ITACHI vectors for highly efficient CRISPR/cas9-mediated gene knockout in *Arabidopsis thaliana*. *Plant Cell Physiol.* 2016;58(1):46–56. <https://doi.org/10.1093/pcp/pcw191>
- Turchetto-Zolet AC, Maraschin FS, de Moraes GL, Cagliari A, Andrade CMB, Margis-Pinheiro M, Margis R. Evolutionary view of acyl-CoA diacylglycerol acyltransferase (DGAT), a key enzyme in neutral lipid biosynthesis. *BMC Evol Biol.* 2011;11(1):263. <https://doi.org/10.1186/1471-2148-11-263>
- Vallochi AL, Teixeira L, da Silva Oliveira K, Maya-Monteiro CM, Bozza PT. Lipid droplet, a key player in host-parasite interactions. *Front Immunol.* 2018;9:1022. <https://doi.org/10.3389/fimmu.2018.01022>
- Vanhercke T, Dyer JM, Mullen RT, Kilaru A, Rahman MM, Petrie JR, Green AG, Yurchenko O, Singh SP. Metabolic engineering for enhanced oil in biomass. *Prog Lipid Res.* 2019;74:103–129. <https://doi.org/10.1016/j.plipres.2019.02.002>
- Vanhercke T, El Tahchy A, Shrestha P, Zhou X-R, Singh SP, Petrie JR. Synergistic effect of WRI1 and DGAT1 coexpression on triacylglycerol biosynthesis in plants. *FEBS Lett.* 2013;587(4):364–369. <https://doi.org/10.1016/j.febslet.2012.12.018>
- van Wijk KJ, Kessler F. Plastoglobuli: plastid microcompartments with integrated functions in metabolism, plastid developmental transitions, and environmental adaptation. *Annu Rev Plant Biol.* 2017;68(1):253–289. <https://doi.org/10.1146/annurev-arplant-043015-111737>
- Vidi P-A, Kanwischer M, Baginsky S, Austin JR, Csucs G, Dörmann P, Kessler F, Bréhélin C. Tocopherol cyclase (VTE1) localization and vitamin E accumulation in chloroplast plastoglobule lipoprotein particles. *J Biol Chem.* 2006;281(16):11225–11234. <https://doi.org/10.1074/jbc.M511939200>
- Wang L, Shen W, Kazachkov M, Chen G, Chen Q, Carlsson AS, Szymne S, Weselake RJ, Zou J. Metabolic interactions between the lands cycle and the Kennedy pathway of glycerolipid synthesis in *Arabidopsis* developing seeds. *Plant Cell.* 2012;24(11):4652–4669. <https://doi.org/10.1105/tpc.112.104604>
- Wang W, Wen Y, Berkey R, Xiao S. Specific targeting of the *Arabidopsis* resistance protein RPW8.2 to the interfacial membrane encasing the fungal haustorium renders broad-spectrum resistance to powdery mildew. *Plant Cell.* 2009;21(9):2898–2913. <https://doi.org/10.1105/tpc.109.067587>
- Welti R, Li W, Li M, Sang Y, Biesiada H, Zhou H-E, Rajashekar CB, Williams TD, Wang X. Profiling membrane lipids in plant stress responses. Role of phospholipase D alpha in freezing-induced lipid changes in *Arabidopsis*. *J Biol Chem.* 2002;277(35):31994–32002. <https://doi.org/10.1074/jbc.M205375200>
- Weng H, Molina I, Shockey J, Browse J. Organ fusion and defective cuticle function in a *lacs1 lacs2* double mutant of *Arabidopsis*. *Planta.* 2010;231(5):1089–1100. <https://doi.org/10.1007/s00425-010-1110-4>
- Weßling R, Panstruga R. Rapid quantification of plant-powdery mildew interactions by qPCR and conidiospore counts. *Plant Methods.* 2012;8(1):35. <https://doi.org/10.1186/1746-4811-8-35>
- Wildermuth MC. Modulation of host nuclear ploidy: a common plant biotroph mechanism. *Curr Opin Plant Biol.* 2010;13(4):449–458. <https://doi.org/10.1016/j.pbi.2010.05.005>
- Wildermuth MC, Steinwand MA, McRae AG, Jaenisch J, Chandran D. Adapted biotroph manipulation of plant cell ploidy. *Annu Rev Phytopathol.* 2017;55(1):537–564. <https://doi.org/10.1146/annurev-phyto-080516-035458>
- Winter D, Vinegar B, Nahal H, Ammar R, Wilson GV, Provart NJ. An ‘electronic fluorescent pictograph’ browser for exploring and analyzing large-scale biological data sets. *PLoS One.* 2007;2(8):e718. <https://doi.org/10.1371/journal.pone.0000718>
- Xu C, Fan J, Shanklin J. Metabolic and functional connections between cytoplasmic and chloroplast triacylglycerol storage. *Prog Lipid Res.* 2020;80:101069. <https://doi.org/10.1016/j.plipres.2020.101069>
- Xu C, Shanklin J. Triacylglycerol metabolism, function, and accumulation in plant vegetative tissues. *Annu Rev Plant Biol.* 2016;67(1):179–206. <https://doi.org/10.1146/annurev-arplant-043015-111641>
- Xu X-Y, Yang H-K, Singh SP, Sharp PJ, Liu Q. Genetic manipulation of non-classic oilseed plants for enhancement of their potential as a bioreactor for triacylglycerol production. *Engineering.* 2018;4(4):523–533. <https://doi.org/10.1016/j.eng.2018.07.002>
- Xue J, Gao H, Xue Y, Shi R, Liu M, Han L, Gao Y, Zhou Y, Zhang F, Zhang H, et al. Functional characterization of soybean diacylglycerol acyltransferase 3 in yeast and soybean. *Front Plant Sci.* 2022;13:854103. <https://doi.org/10.3389/fpls.2022.854103>
- Yan B, Xu X, Gu Y, Zhao Y, Zhao X, He L, Zhao C, Li Z, Xu J. Genome-wide characterization and expression profiling of diacylglycerol acyltransferase genes from maize. *Genome.* 2018;61(10):735–743. <https://doi.org/10.1139/gen-2018-0029>
- Yao H-Y, Lu Y-Q, Yang X-L, Wang X-Q, Luo Z, Lin D-L, Wu J-W, Xue H-W. *Arabidopsis* Sec14 proteins (SFH5 and SFH7) mediate inter-organelle transport of phosphatidic acid and regulate chloroplast development. *Proc Natl Acad Sci U S A.* 2023;120(6):e2221637120. <https://doi.org/10.1073/pnas.2221637120>
- Yin X, Guo X, Hu L, Li S, Chen Y, Wang J, Wang RR-C, Fan C, Hu Z. Genome-wide characterization of DGATs and their expression diversity analysis in response to abiotic stresses in *Brassica napus*. *Plants.* 2022;11(9):1156. <https://doi.org/10.3390/plants11091156>
- Ytterberg AJ, Peltier J-B, van Wijk KJ. Protein profiling of plastoglobules in chloroplasts and chromoplasts. A surprising site for differential accumulation of metabolic enzymes. *Plant Physiol.* 2006;140(3):984–997. <https://doi.org/10.1104/pp.105.076083>

- Zhang M, Fan J, Taylor DC, Ohlrogge JB. DGAT1 and PDAT1 acyltransferases have overlapping functions in Arabidopsis triacylglycerol biosynthesis and are essential for normal pollen and seed development. *Plant Cell*. 2009;21(12):3885–3901. <https://doi.org/10.1105/tpc.109.071795>
- Zhang R, Wise RR, Struck KR, Sharkey TD. Moderate heat stress of *Arabidopsis thaliana* leaves causes chloroplast swelling and plastoglobule formation. *Photosynth Res*. 2010;105(2):123–134. <https://doi.org/10.1007/s11120-010-9572-6>
- Zhao L, Katavic V, Li F, Haughn GW, Kunst L. Insertional mutant analysis reveals that long-chain acyl-CoA synthetase 1 (LACS1), but not LACS8, functionally overlaps with LACS9 in Arabidopsis seed oil biosynthesis. *Plant J*. 2010;64(6):1048–1058. <https://doi.org/10.1111/j.1365-313X.2010.04396.x>
- Zhou X-R, Bhandari S, Johnson BS, Kotapati HK, Allen DK, Vanhercke T, Bates PD. Reorganization of acyl flux through the lipid metabolic network in oil-accumulating tobacco leaves. *Plant Physiol*. 2020;182(2):739–755. <https://doi.org/10.1104/pp.19.00667>
- Zhou X-R, Shrestha P, Yin F, Petrie JR, Singh SP. AtDGAT2 is a functional acyl-CoA:diacylglycerol acyltransferase and displays different acyl-CoA substrate preferences than AtDGAT1. *FEBS Lett*. 2013;587(15):2371–2376. <https://doi.org/10.1016/j.febslet.2013.06.003>